

Award Accounts

The Chemical Society of Japan Award for Young Chemists for 2003

Multiphoton Chemical Reactions on Liquid Beam Surfaces

Jun-ya Kohno,* Fumitaka Mafuné,† and Tamotsu Kondow

East Tokyo Laboratory, Genesis Research Institute, Inc. and Cluster Research Laboratory, Toyota Technological Institute, 717-86 Futamata, Ichikawa, Chiba 272-0001

Received September 7, 2004; E-mail: kohno@clusterlab.jp

In this account, we describe the dynamics of reactions induced by multiphoton excitation of solute and solvent molecules in solutions, studied by means of a liquid beam (a continuous liquid flow in a vacuum) combined with mass spectrometry. Unique reaction intermediates and products are found to be produced and ejected into the gas phase by multiphoton excitation of the molecules in the liquid beam. The reaction dynamics were elucidated by observing the reaction intermediates and products ejected into the gas phase. In particular, we refer to reactions via UV multiphoton excitation of solute molecules, such as ketal formation of phenyl ketones and reduction by solvated electrons, and those via IR multiphoton excitation of solvent molecules, such as formation of internally hot and cold molecules/clusters in the gas phase.

Reactions of molecules in solutions are characterized by how the molecules are excited. Thermal excitation drives most of the conventional chemical reactions, where excitation energy is apportioned among the molecules in the solution in a statistical manner. Photoexcitation by light also initiates unique chemical reactions, where a molecule of interest is selectively excited into a specific excited state under irradiation of light with an appropriate wavelength and an intensity. In this account, we describe particularly photochemical reactions under irradiation of an intense laser in solutions, in which more than one photon are involved. These photochemical reactions should be called "multiphoton chemical reactions".

Reactant solute molecules in a solution are excited by absorbing one or more photons into reaction intermediates under irradiation of an intense laser. It is highly probable that the reaction intermediates further absorb one or more photons into unique reaction products, which are not formed in conventional photochemical reactions. The photochemical reactions initiated by the multiphoton absorption, i.e. multiphoton chemical reactions, are essentially different from the conventional photochemical reactions, because new photochemical reaction channels are opened through excitation of the reaction intermediates. The multiphoton chemical reactions have been explored by Scaiano and his co-workers, who have analyzed reaction products formed by shining pulsed UV lasers to solutions.[1–4] They have shown, for example, that various biradical intermediates are generated in the solutions by two photon excitation and initiate novel reactions which are totally different from those produced by conventional photochemical reactions. Wilson and his co-workers have obtained large quantities of multiphoton reaction products by employing a CW argon ion laser.[5,6] Srinivasan and his co-workers have produced carbon and some hydrocarbons as a result of two-photon absorption during ablation of liquid benzene by a pulsed UV laser.[7] This reaction has been further investigated by the other groups.[8,9] Chemical reactions involving multiphoton ionization in solutions have also been studied.[10–16] Belbruno and his co-workers have reported that phenoxy cations are produced as a reaction intermediate both in nitrobenzene and phenol solutions in hexane by irradiation of a pulsed UV laser, and further react into phenoxyphenol and hexyloxyphenol as final products.[10–13] Scaiano and his co-workers have elucidated that photoionization of diphenylmethyl radical is involved in the multiphoton chemical reactions of 1,1-diphenylacetone.[14]

Solvent molecules in solutions also play an important role in the multiphoton chemical reactions, even though the solvent molecules are not directly involved in the reactions. A typical example of such reactions is a matrix assisted laser desorption/ionization (MALDI) which takes advantage of laser excitation of the solvent matrix molecules surrounding the molecules of interest;[17–20] practically MALDI is a powerful technique used for isolation of large molecules into the gas phase with multiphoton excitation of the matrix. Similarly, solvent molecules in a solution in a form of a liquid beam (a thin laminar flow of a liquid in the vacuum) undergo multiphoton excitation which causes solute molecules to be liberated into the gas phase under irradiation of an intense IR laser. This process has been studied, for instance, by Brutschy and his co-workers,

† Present address: Department of Basic Science, Graduate School of Arts and Sciences, The University of Tokyo, Komaba, Meguro-ku, Tokyo 135-8902

Published on the web June 6, 2005; DOI 10.1246/bcsj.78.957

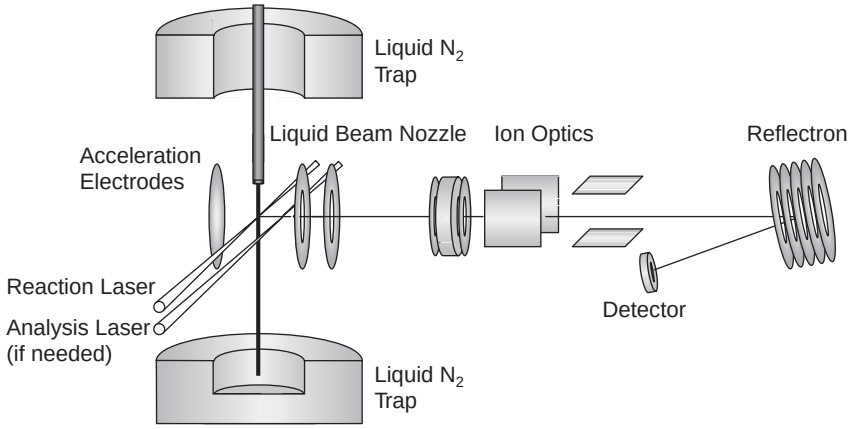

Fig. 1. Schematic diagram of a liquid beam apparatus.

who have investigated multiphoton ionization by an IR laser and have developed a LILBID (laser-induced liquid-beam ionization/desorption) method for isolation of biology-related molecules into the gas phase for mass-spectroscopic identification.[21–27] Abel and his co-workers have recently produced protonated amino acids by shining an IR laser onto the liquid beam of their aqueous solutions.[28,29]

The mechanism of a multiphoton chemical reaction in a solution can be elucidated by taking advantage of reaction intermediates in the solution; a mass spectrometric characterization enables us to determine the reaction intermediates ejected from a solution prepared in a vacuum under irradiation of a laser. Various methods to prepare the surface of a liquid in the vacuum have been elaborated for the investigations of geometrical and electronic structures of the liquid surface.[30–38] A rotating disk method developed by Nathanson and his co-workers is one of the useful methods; here a rotating disk is wetted with a practically non-volatile liquid. Furlan have investigated multiphoton chemical reactions occurring on such liquid surfaces by mass analysis of the species ejected from the surface of the wetted disk.[39,40] The surface of even a volatile liquid can be prepared in the vacuum by use of the liquid-beam technique described above.[41–46,49,50] Faubel and his co-workers have investigated evaporation dynamics of molecules from the surface of a liquid beam,[41,42] and have studied the electronic structures of molecules on various liquid surfaces by means of photoelectron spectroscopy.[43–46] Buntine and his co-workers have applied the liquid-beam technique to chemical analysis.[47,48]

We have investigated multiphoton chemical reactions occurring in the vicinity of a solution surface by irradiation of a pump laser on the surface of the solution introduced into the vacuum as a form of a liquid beam. Ionic and neutral species ejected into the gas phase are identified mass-spectroscopically; a probe UV laser is used when neutral species are to be detected.[49,50] We have revealed the mechanism of ion ejection from the liquid surfaces into the gas phase,[51–54] the solvation structure in the vicinity of the surfaces,[55–57] and the multiphoton chemical reactions following UV multiphoton excitation of solute molecules and IR laser multiphoton excitation of solvent molecules in the vicinity of the solution surfaces.[58–78] We herein describe the chemical reactions following selective multiphoton excitation of solute or solvent molecules in a liquid beam.

1. Instrumentation

A schematic diagram of the apparatus is shown in Fig. 1. A continuous laminar liquid flow (liquid beam) is formed by injecting a liquid into a vacuum chamber through a nozzle having an aperture with 20 μm in diameter. The continuous liquid flow is supplied by a pump designed for a liquid chromatograph. The flow rate is maintained at 0.2 mL/min with a stagnation pressure of typically 20 atm inside the pump. The source chamber is evacuated by a 1200 $L\,s^{-1}$ diffusion pump and a liquid N_2 trap to attain a pressure down to 10^{-4}–10^{-5} Torr during injection of the liquid beam; here the product species are not degraded by any further reactions or collisions with the residual gas. After traveling a distance of ~2 mm from the nozzle, the liquid beam is crossed with a pulsed laser (UV or IR) which initiates multiphoton reactions in the first acceleration region of the TOF mass spectrometer. The other UV laser is focused outside the liquid beam with a certain delay time from the firing of the initial laser when neutral products are of interest. Pulsed nanosecond lasers are more appropriate in the studies because their high peak power facilitates the initiation of multiphoton processes. The UV laser (220–270 nm) is obtained by frequency-doubling the output of a dye laser pumped by the third harmonic of a Nd:YAG laser. In addition, two IR lasers are employed in our studies: (1) a 1.9-μm laser emitted from a Raman shifter filled with 12 atm of H_2 gas as the first Stokes line of the fundamental output of a Nd:YAG laser; and (2) an IR–OPO laser which emits an intense IR radiation with a wavelength of ~3 μm.

The mass-to-charge ratios, m/z, of the product ions are analyzed by a reflectron TOF mass spectrometer. The ions are steered and focused by a set of vertical and horizontal deflectors and an einzel lens. Traveling in a 1.5-m field-free flight tube, the ions are reversed by a reflectron which provides a reversing field tilted by 8° off the beam axis. A train of spatially mass-selected ions are detected by a Daly detector[79,80] after traveling through another 0.5-m field-free region. Signals are amplified and processed by a digital oscilloscope based on a microcomputer. The mass resolution (defined as $m/\Delta m$) range is 70–200 according to the experimental conditions used.

2. Multiphoton Chemical Reactions of Solute Molecules

Reaction intermediates are generated on the liquid-beam

surface of a solution by multiphoton excitation, and react with ambient solute and solvent molecules. Even the reaction intermediates emerging during the course of the reaction are readily ejected into the gas phase together with the products, because these species that are incompletely solvated on the solution surface are not strongly bound to the solvent molecules. Ready detection of such reaction intermediates facilitates elucidation of the reaction mechanism.

In this section, we describe chemical reactions initiated by multiphoton excitation of solute molecules in the vicinity of the solution surface. At the first place, we explain how photoions are ejected from the liquid-beam surface, and then we exemplify a ketal-formation reaction from phenyl ketones and a reduction reaction by solvated electron(s), as the representatives of the chemical reactions initiated by multiphoton excitation of solute molecules in solutions.

2.1 Ion-Ejection Mechanisms from Liquid-Beam Surfaces.[54] Ions produced by a multiphoton ionization of solute molecules are ejected from a liquid surface into the gas phase. The ejection mechanism is explained by a Coulomb-ejection model: In brief, electrons produced simultaneously with the multiphoton ionization are liberated from the liquid surface, leaving electron-depleted layers or positively charged layers. If a repulsive Coulomb energy built by the positive charges surpasses the solvation energy of the ion, it is ejected from the liquid surface to the gas phase.[51–54]

The Coulomb-ejection model is verified by a simultaneous observation of ions ejected from the liquid beam (A_{gas}) by means of a TOF mass spectrometer and those remaining inside the liquid beam (A_{liquid}) probed by an inductive detector. Figure 2a shows A_{gas} and A_{liquid} produced by irradiation by a 266-nm UV laser on a 0.2-M aniline solution in 1-propanol as a function of the laser power. The aniline molecule is employed as an ionization chromophore. As the laser power increases, A_{liquid} increases rapidly and then levels off at a laser power of ~25 μJ/pulse while A_{gas} rises at 25 μJ/pulse and increases gradually. Even though the ions are generated inside the liquid beam by the laser irradiation, no cluster ions in the gas phase are observed until the laser power exceeds a threshold value, ~25 μJ/pulse. The presence of the threshold laser power implies that cluster ions are not ejected until a certain amount of positive ions are piled up on the surface.

The values of A_{gas} and A_{liquid} calculated by using the Coulomb ejection model agree well with those measured experimentally. Let us assume that the solute molecules are dissolved homogeneously in a cylindrical liquid beam with a radius r_0, and that a density $D(r)$ of excess positive charges resulting from the photoionization and subsequent electron liberation in the vicinity of the surface decreases exponentially with the depth from the liquid surface, $r_0 - r$. The density, $D(r)$, is expressed as

$$D(r) = D_0 \exp(-(r_0 - r)/R). \quad (1)$$

Here r is a radial distance from the center of the liquid beam, D_0 is the density of the ions on the liquid surface, and R is the escape depth of an electron produced concurrently with ion formation (see Fig. 3). The exponential decrease of $D(r)$ with $r_0 - r$ is rationalized by the fact that the escape probability of an electron decreases exponentially with the depth. In the Coulomb-ejection model, ions on the surface are considered to be ejected out of the liquid beam from a region where $D(r)$ exceeds the threshold ion density, D_{th}. We assume that all

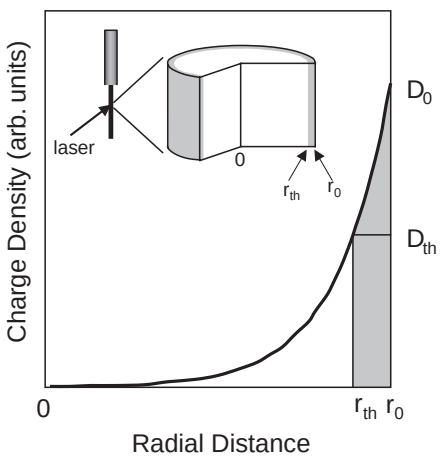

Fig. 3. Charge density inside a liquid beam after UV laser irradiation as a function of a radial distance from the center of the liquid beam.

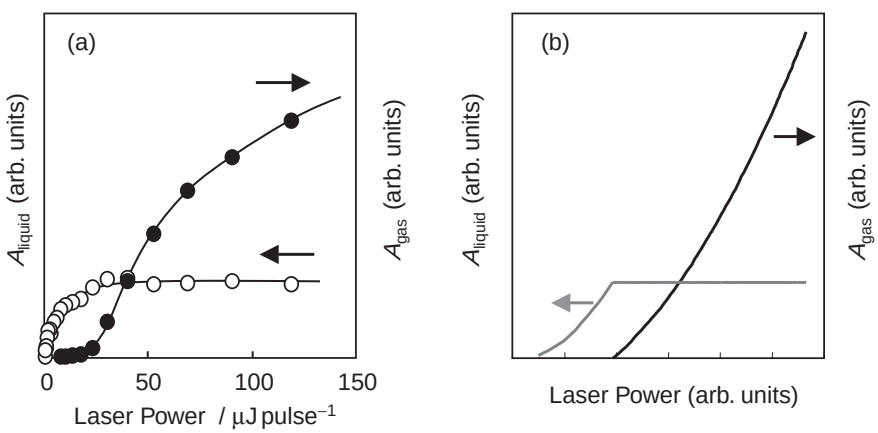

Fig. 2. (a) Intensity, A_{liquid} (open circles), of ions remaining inside the liquid beam of 0.2-M aniline solution in 1-propanol, and that, A_{gas} (solid circle), of cluster ions ejected into the gas phase produced by laser irradiation as a function of the laser power. (b) Intensities, A_{liquid} and A_{gas} calculated by using the Coulomb-ejection model.

the ions in the $r > r_{th}$ region are ejected into the gas phase, and that the ions in the $r < r_{th}$ region are left inside the liquid beam, where $D_{th} = D(r_{th})$, because the ion is likely to diffuse at a slower rate than the ion ejection. On the other hand, the charge density, D_0, on the surface is related to the laser power, I, with a constant, k, as

$$D_0 = kI^2, \tag{2}$$

because the solute molecules (aniline molecules in the present study) are ionized by absorbing two photons. On the basis of the model, the number of ions remaining inside the liquid beam and that ejected into the gas phase are calculated by integrating the number of the ions in a region where the ions are born. Figure 2b shows the calculated ion-abundance inside the liquid beam and that into the gas phase as a function of the laser power. A comparison of Figs. 2a and 2b allows one to conclude that the Coulomb explosion model successfully explains ejection of the ions from the liquid beam surface under irradiation of the laser.

2.2 Ion-Molecule Reactions of Phenyl Ketones.[58,59] In this section, we describe chemical reactions initiated by multiphoton excitation of phenyl ketone in alcohol solutions. It is well known that, in an alcohol solution, a solute phenyl ketone molecule upon photoexcitation to T_1 state abstracts one hydrogen atom from a solvent alcohol molecule into a ketyl radical, which undergoes dimerization.[81] Under irradiation of an intense UV laser, the ketyl radical absorbs more photons to be ionized into a protonated phenyl ketone molecule that is likely to react with alcohol molecules to form a ketal. The reaction mechanism is determined by observing the ionic reaction intermediates ejected from the liquid beam surfaces.

2.2.1 Ketal Formation: Figure 4 shows a typical TOF mass spectrum of ions produced from a 0.5-M solution of acetophenone, $C_6H_5COCH_3$, in ethanol by irradiation of a 250-nm laser. In this spectrum, one intense peak appears at $m/z = 149$ together with other small peaks. The mass number of this intense peak agrees with the sum of the mass numbers of acetophenone ($m/z = 120$) and of ethyl group ($m/z = 29$), which are identified as $C_6H_5C(OC_2H_5)CH_3^+$. The mass assignment is confirmed by the change in a mass number with replacement of a CH_3 group in acetophenone to H or a C_2H_5 group or that of a C_2H_5 group in ethanol to a CH_3 or C_3H_7 group. Namely, the intense peak is assignable to an ion produced by a reaction of one acetophenone molecule and one ethanol molecule. The small peaks in the mass spectrum, on the other hand, are assignable to $C_6H_5C(OH)CH_3^+ \cdot (C_2H_5OH)_n$ ($n \geq 0$) and $C_6H_5C(OCH_3)CH_3^+ \cdot (C_2H_5OH)_n$ ($n \geq 0$).

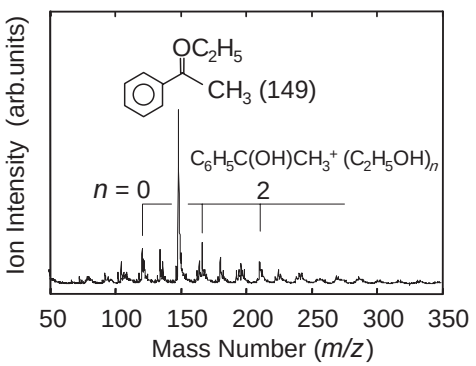

Fig. 4. Typical TOF mass spectrum of ions produced from a 0.5-M solution of acetophenone ($C_6H_5COCH_3$) in ethanol by irradiation of a 250-nm laser.

An acetophenone molecule is excited to T_1 state via S_n state under irradiation of an UV laser. The acetophenone molecule in T_1 state is known to abstract a hydrogen atom from a solvent alcohol molecule into a ketyl radical, $C_6H_5\dot{C}(OH)CH_3$.[81] The ketyl radical is dimerized under irradiation of light with a moderate intensity, whereas the ketyl radical further absorbs more photons into $C_6H_5C(OH)CH_3^+$ under irradiation of an intense UV laser. Small peaks in the mass spectrum given in Fig. 4 are assignable to the ions produced by further absorption of photons. The ion, $C_6H_5C(OH)CH_3^+$, is identified as a protonated acetophenone known as a reaction intermediate of a ketal formation, which occurs by adding acids to the solution. In $C_6H_5C(OH)CH_3^+$, the carbon atom bonded to the OH group is positively charged, and is readily attacked by the oxygen atom of an ethanol molecule having a lone-pair electrons as a nucleophile to result into a ketal ion, $C_6H_5C(OC_2H_5)CH_3^+$. The ketal ion, $C_6H_5C(OC_2H_5)CH_3^+$, is observed as the most intense peak in the mass spectrum. In summary, multiphoton excitation of an acetophenone molecule in an ethanol solution initiates the ketal-formation reaction which gives a ketal ion, $C_6H_5C(OC_2H_5)CH_3^+$, via a protonated acetophenon, $C_6H_5C(OH)CH_3^+$. The reaction mechanism is summarized in Scheme 1.

In the reaction of protonated phenyl ketones, $C_6H_5C(OH)R^+$, with alcohols, the reactivity is expected to decrease with an increase of the geometrical size of R. Figure 5 shows typical mass spectra of ions produced from C_6H_5COR (R = H, C_2H_5, and C_6H_5) in ethanol solutions. As shown in Fig. 5, the relative abundance of the product ion, $C_6H_5C(OC_2H_5)R^+$ with respect to that of $C_6H_5C(OH)R^+$ decreases with the geometrical size of R. Namely, the relative abundance imitates the rate constant of the reaction concerned.

2.2.2 Competition between Ketal and Pinacol Formation: Figure 6 shows a typical mass spectrum of ions produced from a 0.5-M solution of benzophenone, $C_6H_5COC_6H_5$, in ethanol by irradiation of a 250-nm laser. In this spectrum, $C_6H_5C(OH)C_6H_5^+ \cdot (C_2H_5OH)_n$ and $C_6H_5C(OC_2H_5)C_6H_5^+ \cdot (C_2H_5OH)_n$ are observed in a low mass region. In addition,

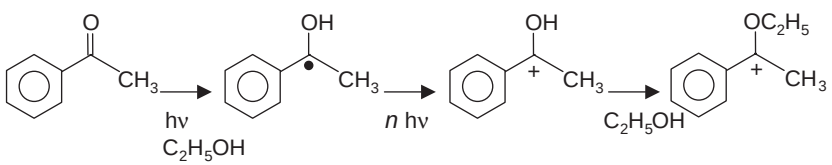

Scheme 1.

pinacol ions, $[C_6H_5C(OH)C_6H_5]_2^+ \cdot (C_2H_5OH)_n$, are observed in a high mass region; these are produced by a dimerization reaction of ketyl radicals, followed by photoionization in the vicinity of the solution surface. Figures 7a and 7b show the abundance of the product ions as functions of the concentration of benzophenone in the ethanol solution and of the power of the irradiation laser, respectively. As the laser power increases, the abundance of the pinacol ion starts to rise at a threshold laser power and tends to level off after passing through a slight maximum, while the abundance of the pinacol ion does not change with the concentration. These tendencies are contrasted to those of the protonated benzophenone ion: the abundance of the protonated benzophenone ion continues to increase with increase in the laser power and with the concentration of benzophenone.

The pinacol ions are not produced from alcohol solutions of benzaldehyde, acetophenone, and propiophenone but are produced from an alcohol solution of benzophenone (see for example, Fig. 4), probably because of inhomogeneous solvation of benzophenone on the ethanol solution surface. The phenyl ketones other than benzophenone are considered to have a low probability of a bimolecular encounter of the ketyl radicals in the time window of the photoionization (<10 ns). The pinacol ion could be observed when the time window of photoionization is sufficiently long or the probability of a bimolecular encounter is sufficiently large. Namely, the rate of the bimolecular encounter of benzophenone must be larger than that of the

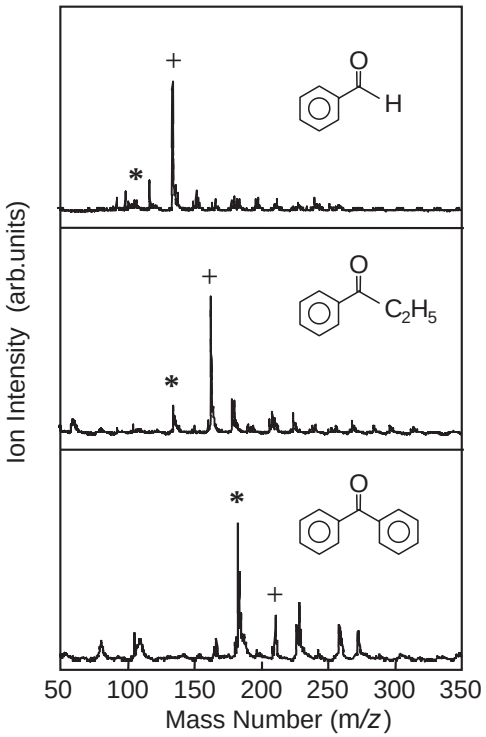

Fig. 5. TOF mass spectra of ions produced from 0.5-M ethanol solutions of benzaldehyde, propiophenone, and benzophenone (C_6H_5COR, R = H, C_2H_5, C_6H_5) by irradiation of a 250-nm laser. The reactant ions ($C_6H_5C(OH)R^+$ (marked with ∗)) are observed in the spectra together with the product ions ($C_6H_5C(OC_2H_5)R^+$ (marked with +)).

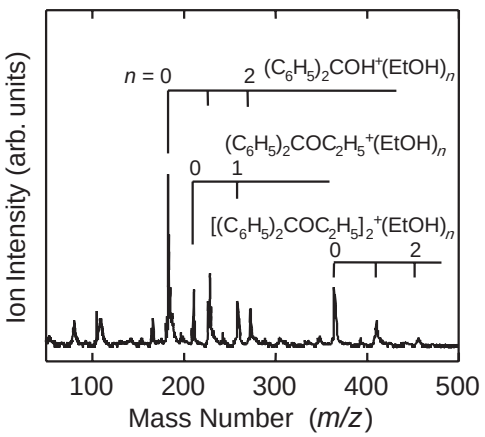

Fig. 6. TOF mass spectrum of ions produced from a 0.5-M solution of benzophenone ($C_6H_5COC_6H_5$) in ethanol by irradiation of a 250-nm laser.

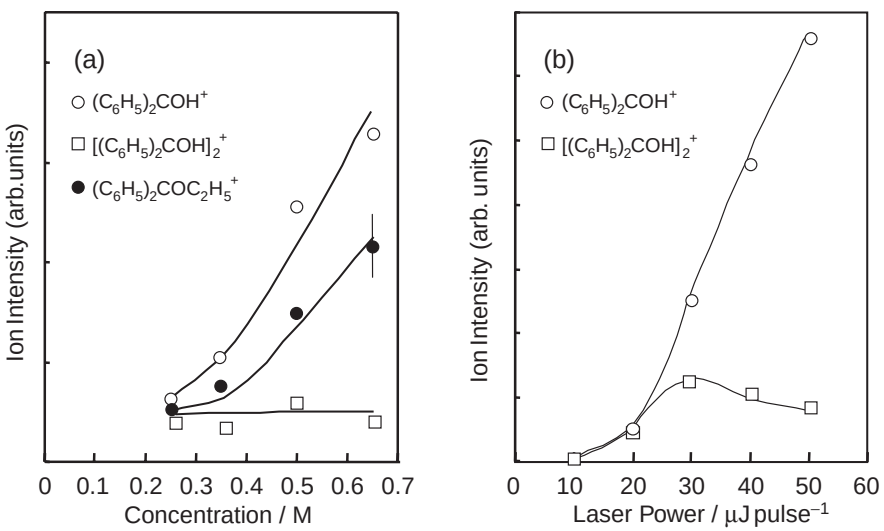

Fig. 7. Intensities of product ions as functions of (a) the concentration of benzophenone in an ethanol solution and (b) the laser power.

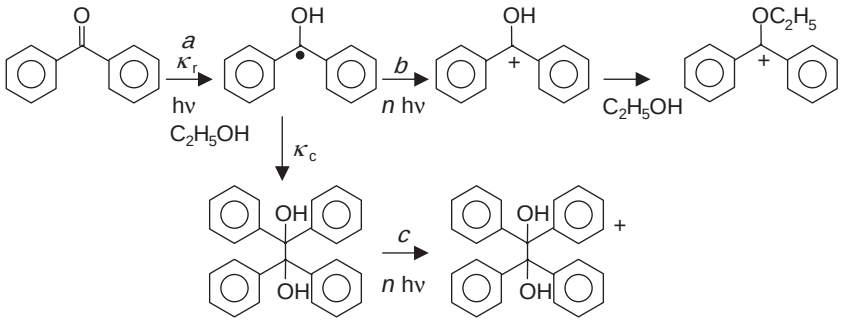

Scheme 2.

other phenyl ketones. If the ketyl radicals are homogeneously distributed in the vicinity of the solution surface, the probability of the bimolecular encounter is considered to be almost the same for all the ketyl radicals studied. It is considered that benzophenone dimers are initially present in the vicinity of the solution surface and serve as precursors of the pinacol-formation reaction. The concentration of the dimer precursor seems to be independent of the solute concentration as shown in Fig. 7a. Seemingly, a high concentration of the benzophenone dimer on the ethanol solution surface is explained by the two hydrophobic phenyl groups which cause themselves to orient outside the surface because of a hydrophilic nature of the alcohol.

The laser-power dependence shown in Fig. 7b is explained in terms of a simple kinetic model: (1) a benzophenone molecule (B) is excited into T_1 state (B^*) by absorbing one photon; (2) B^* abstracts one hydrogen atom from an alcohol molecule (ROH) into a ketyl radical ($\dot{B}H$); (3) $\dot{B}H$ is either dimerized into pinacol and then is ionized, or is ionized before the dimerization. The processes are expressed as

$$B + h\nu \rightarrow B^*, \tag{3}$$

$$B^* + ROH \rightarrow \dot{B}H + \dot{R}O, \tag{4}$$

$$\dot{B}H + 2h\nu \rightarrow BH^+, \tag{5}$$

$$2\dot{B}H \rightarrow (BH)_2, \tag{6}$$

$$(BH)_2 + 2h\nu \rightarrow (BH)_2{}^+. \tag{7}$$

As stated, the benzophenone molecules form the dimer precursor, where the rate of the dimerization (process 6) as well as the hydrogen abstraction (process 4) is sufficiently high that these reactions proceed in the time window of the photoionization. Under these circumstances, one can assume the steady state condition for [B^*], [$\dot{B}H$], and [$(BH)_2$], obtaining the relations

$$\frac{d[B^*]}{dt} = aI[B] - \kappa_r[B^*][ROH] = 0, \tag{8}$$

$$\frac{d[\dot{B}H]}{dt} = \kappa_r[B^*][ROH] - bI^2[\dot{B}H] - \kappa_c[\dot{B}H]^2 = 0, \tag{9}$$

$$\frac{d[(BH)_2]}{dt} = \kappa_c[\dot{B}H]^2 - cI^2[(BH)_2] = 0, \tag{10}$$

where the bracket designates the number density of the species given in the bracket, a is the absorption coefficient of benzophenone, I is the laser power, κ_r is the rate constant for the hydrogen abstraction reaction (process 4), b is the coefficient for the photoionization of ketyl radical (process 5), κ_c is the rate constant for the dimerization reaction (process 6), and c is the coefficient for the photoionization (process 7) (see Scheme 2). By solving these relations, one can obtain [$\dot{B}H$] and [$(BH)_2$]. The ion abundances, [BH^+] and [$(BH)_2{}^+$] are considered to be proportional to $bI^2[\dot{B}H]$ and $cI^2[(BH)_2]$, respectively, because these ionic species are produced by two photon absorption. Let us solve Eqs. 8–10 under such an extreme condition that the laser power is either sufficiently large or small. If the laser power is sufficiently small, $\kappa_c[\dot{B}H]^2$ is considered to be larger than $bI^2[\dot{B}H]$. Hence, Eq. 9 is reduced to

$$\kappa_r[B^*][ROH] - \kappa_c[\dot{B}H]^2 = 0. \tag{11}$$

By solving Eqs. 8, 10, and 11, one obtains the laser-power dependence to be

$$[BH^+] \propto \frac{b(a[B])^{1/2}}{\sqrt{\kappa_c}} I^{5/2}, \tag{12}$$

$$[(BH)_2{}^+] \propto a[B]I. \tag{13}$$

On the other hand, if the laser power is sufficiently large, $bI^2[\dot{B}H]$ is considered to be larger than $\kappa_c[\dot{B}H]^2$. Hence, Eq. 9 is reduced to

$$\kappa_r[B^*][ROH] - bI^2[\dot{B}H] = 0. \tag{14}$$

By solving Eqs. 8, 10, and 14, one obtains the laser-power dependence to be

$$[BH^+] \propto a[B]I, \tag{15}$$

$$[(BH)_2{}^+] \propto \frac{a^2\kappa_c[B]^2}{b^2} I^{-2}. \tag{16}$$

The laser-power dependence (I-dependence) derived from the model reproduces the experimental results as shown in Fig. 7b: [BH^+] increases with increase in the laser power (Eqs. 12 and 15), while [$(BH)_2{}^+$] increases (Eq. 13) and then decreases (Eq. 16) with increase in the laser power. The decrease of [$(BH)_2$] with the laser power is explained by using this model as follows: The number density of the ketyl radical, [$\dot{B}H$], is proportional to the laser power, and the probability of the bimolecular encounter of $\dot{B}H$ is proportional to $[\dot{B}H]^2$. The increasing photoionization probability of $\dot{B}H$ with the laser power implies that the two competing paths operate for consumption of $\dot{B}H$. When the laser power is relatively small, the probability of the bimolecular encounter is larger than that of the photoionization, whereas the probability of the photoionization sur-

passes that of the bimolecular encounter with the laser power, and as a result, $[(BH)_2{}^+]$ decreases with the laser power.

In summary, we observe a reaction of benzophoenone molecules in an ethanol solution under irradiation of an intense UV laser. A ketal formation via multiphoton excitation proceeds as well as pinacol formation through a regular photochemical reaction. The benzophenone molecule is likely to be solvated inhomogeneously on the solution surface. A kinetic model of the reactions explained the branching ratio of the two reactions as a function of the laser power.

2.3 Chemical Reactions Involving Solvated Electrons.[69,70] Solvated electrons induce unique chemical reactions in a solution, such as selective reduction of aromatic into unsaturated hydrocarbons in the presence of a hydrogen donor.[82] A variety of reactions involving solvated electrons have been investigated so far, and their rate constants have been measured by pulse radiolysis.[83,84] Similar reactions have been investigated by excitation with a laser, where a solvated electrons are produced by excitation of the charge-transfer-to-solvent (CTTS) band[85] of negative ions in solution. In the present study, metal halides in alcohol solutions were used for the investigation of chemical reactions involving solvated electrons because the solvated electrons are conveniently produced from the metal halides under laser irradiation. The mechanisms of the reactions are elucidated through observing ionic reaction intermediates by use of the liquid beam technique. In addition, novel reactions are found to proceed in the presence of many solvated electrons produced by irradiation of a more intense laser. In this section, we describe chemical reactions of solvated electron(s) produced by irradiation of UV laser onto metal halides in alcohol solutions.

2.3.1 Reduction by Solvated Electrons: Upon irradiation of a UV laser on a liquid-beam surface of a metal halide solution, a valence electron of a halide ion, X^-, is released as a solvated electron in the solution due to excitation of the CTTS (Charge Transfer to Solvent) band of X^-.[85] The solvated electron thus produced reacts with surrounding species in the solution. Figure 8 shows typical mass spectra of ions produced by irradiation of a 266-nm laser on a 0.1-M $CaCl_2$ solution in ethanol (EtOH) (panel a) and a 0.1-M $CaCl_2$ solution in a mixture of 3 M chloroform ($CHCl_3$) in ethanol (panel b) in the range between $m/z = 100$ and 150. Peaks in the mass spectra are assigned as $Ca^+\cdot(EtOH)_m$, $CaOEt^+\cdot(EtOH)_m$, $CaOH^+\cdot(EtOH)_m$, $CaCl^+\cdot(EtOH)_m$, and $H^+\cdot(EtOH)_m$. The mass assignment is confirmed by replacement of ethanol with methanol or 1-propanol. By the addition of $CHCl_3$, the peak of $Ca^+\cdot(EtOH)_2$ vanishes, and the peak of $CaOEt^+\cdot(EtOH)_1$ decreases slightly in intensity, while the peaks of $CaCl^+\cdot(EtOH)_1$ and $H^+\cdot(EtOH)_3$ increase in intensity. Figure 9 shows the intensities of $Ca^+\cdot(EtOH)_2$, $CaOEt^+\cdot(EtOH)_1$, $CaCl^+\cdot(EtOH)_1$, and $H^+\cdot(EtOH)_3$ as a function of the concentration of $CHCl_3$ in the 0.1-M $CaCl_2$ solution in ethanol. The intensities of $Ca^+\cdot(EtOH)_2$ and $CaOEt^+\cdot(EtOH)_1$ decrease, and those of $CaCl^+\cdot(EtOH)_1$ and $H^+\cdot(EtOH)_3$ increase as the concentration of $CHCl_3$ increases.

A solute molecule, $CaCl_2$, in an ethanol solution is dissociated into $CaCl^+$ and Cl^-, and further into Ca^{2+} and $2Cl^-$. The Cl^- ions have the CTTS band with the absorption maximum

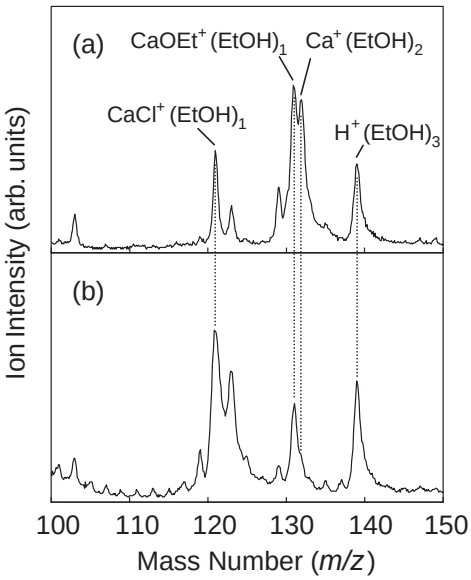

Fig. 8. Mass spectra of ions produced by irradiation of a 266-nm laser on (a) a 0.1-M $CaCl_2$ solution in ethanol and (b) a 0.1-M $CaCl_2$ solution in a mixture of 3-M chloroform ($CHCl_3$) in ethanol in the range between $m/z = 100$ and 150.

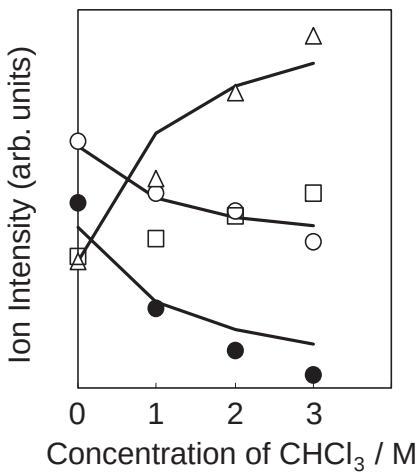

Fig. 9. Intensities of $Ca^+\cdot(EtOH)_2$ (●), $CaOEt^+\cdot(EtOH)_1$ (○), $CaCl^+\cdot(EtOH)_1$ (△), and $H^+\cdot(EtOH)_3$ (□) as a function of the concentration of $CHCl_3$ in the 0.1-M $CaCl_2$ solution in ethanol.

at 185 nm. Since the absorption coefficient is sufficiently large (more than 0.06 $mol^{-1}\,dm^3\,cm^{-1}$) even at the wavelength (266 nm) of the excitation laser, the Cl^- excited into the CTTS state under irradiation of the 266-nm laser releases one electron into the solution as a solvated electron, $e_s{}^-$. This solvated electron is ejected into the gas phase as a free electron by absorbing one more photon in the duration of the same pulse. These processes are expressed as

$$Cl^-(soln) + h\nu \rightarrow Cl^{-CTTS}(soln) \rightarrow Cl(soln) + e_s{}^-(soln), \quad (17)$$

$$e_s{}^-(soln) + h\nu \rightarrow e_f{}^-, \quad (18)$$

where e_f^- is a free electron and (soln) represents solution. Ions such as Ca^+, $CaOEt^+$, $CaCl^+$, and H^+ generated through various processes in the solution are ejected from the liquid surface by Coulomb ejection as described in Section 2.1. In the solution, Ca^{2+} and $CaCl^+$ are initially produced by dissociation of $CaCl_2$ dissolved in the solution, and Ca^{2+} is reduced to Ca^+ by solvated electrons:

$$e_s^- + Ca^{2+}(soln) \rightarrow Ca^+(soln). \quad (19)$$

On the other hand, the core ion, $CaOEt^+$, is produced by association of Ca^{2+} with EtO^- produced by a reaction of a solvated electron, e_s^-, with a solvent molecule in the solution as

$$e_s^- + EtOH(soln) \rightarrow EtO^-(soln) + H(soln), \quad (20)$$

$$Ca^{2+}(soln) + EtO^-(soln) \rightarrow CaOEt^+(soln). \quad (21)$$

Formation of EtO^- by the reaction of e_s^- with EtOH is also observed in an ethanol solution of sodium iodide (NaI).[67]

It is highly likely that Ca^{2+} solvated with EtOH molecules is ejected into the gas phase with several accompanying EtOH molecules as $Ca^{2+}\cdot(EtOH)_n$, which undergoes unimolecular dissociation into $CaOEt^+\cdot(EtOH)_m$ and $H^+\cdot(EtOH)_m$.[68] Larger cluster ions, $Ca^{2+}\cdot(EtOH)_n$ ($m \geq 3$), are not observed because they are not stable and decompose into $CaOEt^+$.[86–88] In short, three parallel mechanisms operate in the production of $CaOEt^+$ (see Scheme 3a): namely, (1) association of Ca^{2+} with EtO^-, (2) intracluster charge transfer in $Ca^{2+}\cdot(EtOH)_n$ in the gas phase and subsequent Coulomb explosion, and (3) intracluster hydrogen elimination in $Ca^+\cdot(EtOH)_m$. In addition, $H^+\cdot(EtOH)_m$ is produced by nonresonant two-photon ionization of solvent ethanol molecules under irradiation of a 266-nm laser on pure ethanol.[61]

With increase in the concentration of $CHCl_3$ in the $CaCl_2$ ethanol solution, the intensities of $Ca^+\cdot(EtOH)_2$ and $CaOEt^+\cdot(EtOH)_1$ decrease, while those of $CaCl^+\cdot(EtOH)_1$ and $H^+\cdot(EtOH)_3$ increase. This result is explained by scavenging solvated electrons by $CHCl_3$ and forming Cl^- and $CHCl_2$. In other words, a lower amount of Ca^+ and $CaOEt^+$ is produced in a higher concentration of $CHCl_3$, because fewer solvated electrons are available for the reaction with Ca^{2+} and EtOH. This electron scavenging reaction of $CHCl_3$ is schematically depicted in Scheme 3b, where the thick line shows the reaction accelerated by the addition of $CHCl_3$ and the dotted line shows the reaction decelerated by this addition.

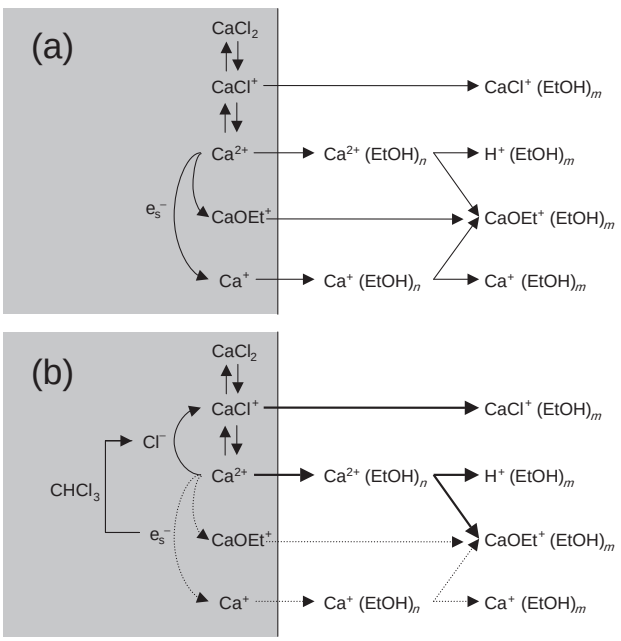

Scheme 3.

2.3.2 Reactions Involving Multi-Solvated Electrons: Chemical reactions involving more than one solvated electrons are studied in a CaI_2 solution in ethanol by observing the ionic species under irradiation of an intense 220-nm laser which excites I^- into CTTS state.

Figures 10a and 10b show mass spectra of ions produced by irradiation of a 220-nm laser on the liquid beam of a 0.5-M CaI_2 solution in ethanol at the power values of 60 μJ/pulse and 130 μJ/pulse, respectively. Peaks in the mass spectrum shown in Fig. 10a are assigned to $CaOEt^+\cdot(EtOH)_m$ ($m = 0$–6), $CaOH^+\cdot(EtOH)_m$ ($m = 0$–2), and $CaI^+\cdot(EtOH)_m$ ($m = 0$–5), which are categorized as Class I hereafter. At a higher laser power, ions beside the cluster ions of Class I gain more intensity, as shown in Fig. 10b. The ions have the mass numbers of $40n + 45i + 17j + 16k + 127l$ ($n = 2, 3, \ldots$, and i, j, k and $l = 0, 1, 2, \ldots$ with the constraint of $2n - i - j - 2k - l = 1$); 40, 45, 17, 16, and 127, which correspond to Ca^{2+}, EtO^-, OH^-, O^{2-}, and I^-, respectively. The constraint, $2n - i - j - 2k - l = 1$, implies that these ions are singly charged, and hence can be assigned as $[Ca_n(OEt)_i(OH)_j(O)_k(I)_l]^+$ (Class II hereafter).

Figure 11 shows the relative abundance, R_X, of a cluster ion containing X (X = EtO^-, OH^-, O^{2-}, and I^-) (Class II) as a function of the laser power. The value, R_X is defined as

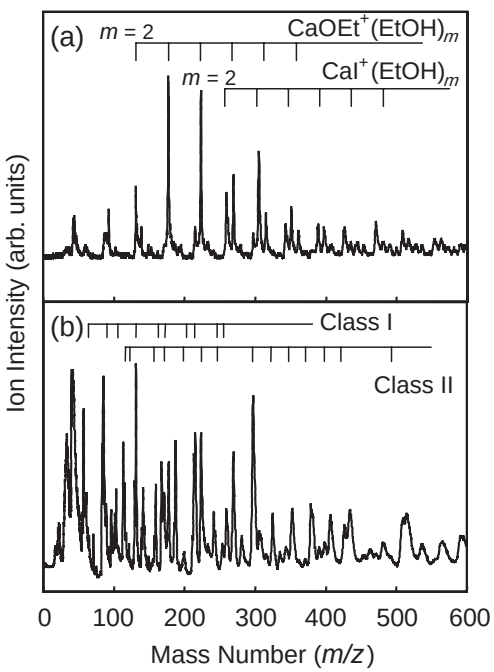

Fig. 10. Mass spectra of ions produced by irradiation of a 220-nm laser on the liquid beam of a 0.5-M CaI_2 solution in ethanol at (a) 60 μJ/pulse and (b) 130 μJ/pulse. Definition of Class I and Class II is given in the text.

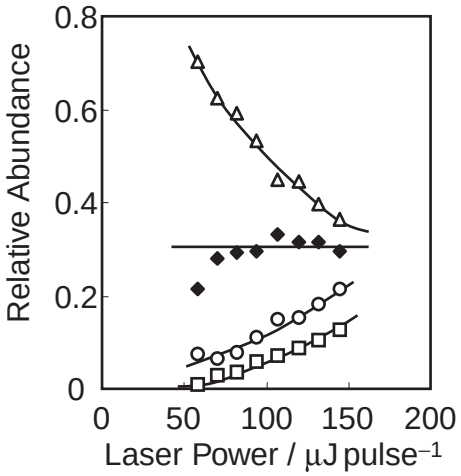

Fig. 11. Relative abundance, R_X, of a cluster ion containing X (X = EtO^- (△), OH^- (○), O^{2-} (●), and I^- (◆)), which belongs to Class II, as a function of the laser power.

$$R_{EtO^-} = \frac{\sum_i iI_{i,j,k,l}}{\sum_i iI_{i,j,k,l} + \sum_j jI_{i,j,k,l} \sum_k kI_{i,j,k,l} + \sum_l lI_{i,j,k,l}}, \quad (22)$$

$$R_{OH^-} = \frac{\sum_i jI_{i,j,k,l}}{\sum_i iI_{i,j,k,l} + \sum_j jI_{i,j,k,l} \sum_k kI_{i,j,k,l} + \sum_l lI_{i,j,k,l}}, \quad (23)$$

$$R_{O^{2-}} = \frac{\sum_i kI_{i,j,k,l}}{\sum_i iI_{i,j,k,l} + \sum_j jI_{i,j,k,l} \sum_k kI_{i,j,k,l} + \sum_l lI_{i,j,k,l}}, \quad (24)$$

$$R_{I^-} = \frac{\sum_i lI_{i,j,k,l}}{\sum_i iI_{i,j,k,l} + \sum_j jI_{i,j,k,l} \sum_k kI_{i,j,k,l} + \sum_l lI_{i,j,k,l}}, \quad (25)$$

where $I_{i,j,k,l}$ designates the intensity of $[Ca_n(OEt)_i(OH)_j(O)_k(I)_l]^+$. As the laser power increases, R_{EtO^-} decreases monotonically, R_{OH^-} and $R_{O^{2-}}$ increase, and R_{I^-} is practically unchanged.

One can explain the formation of a Class-I cluster ion by a mechanism identical to that described in the previous section; a solvated electron reacts with EtOH into EtO^-, which further associates with Ca^{2+} to form $CaOEt^+$. The ion, $CaOH^+$, is produced similarly when OH^- is generated in the intermediate stage. One solvated electron is involved in these association reactions, and hence the abundances of $CaOEt^+$ and $CaOH^+$ increase linearly with the number of the solvated electron (first-order reaction). Practically, no solvated electron is involved in the formation of CaI^+, because the electrolytic dissociation of CaI_2 in the solution provides a dominant amount of CaI^+.

The Class-II cluster ions, $[Ca_n(OEt)_i(OH)_j(O)_k(I)_l]^+$, which are not present originally in the solution, are generated only when the liquid beam is irradiated with an intense laser. Evidently, many solvated electrons are involved in the formation of the Class-II cluster ions, because the Class-II cluster ions contain more than one anion of OEt^-, OH^-, and O^{2-}, which

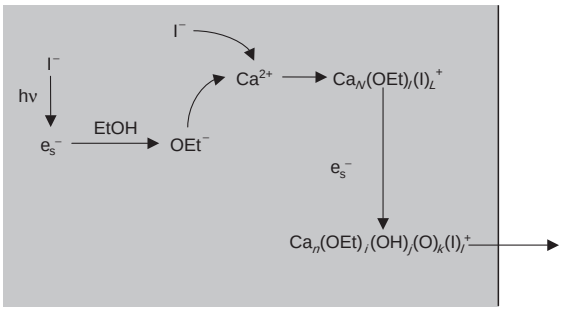

Scheme 4.

are produced from one or more solvated electrons. The formation mechanism of the Class-II cluster ions is inferred from the dependence of the relative abundances of EtO^-, OH^-, O^{2-}, and I^- on the laser power. No substantial change of the I^- abundance with the laser power is consistent with the fact that I^- is always supplied from the dissociation of CaI_2. On the other hand, the relative abundance of EtO^- decreases, while those of OH^- and O^{2-} increase as the laser power increases. Radiolysis studies have revealed that EtO^- is the primary product of the reaction of a solvated electron with an ethanol molecule. Taking advantage of this finding, one may conclude that the primary product of the present reaction is $[Ca_N(OEt)_I(I)_L]$, which reacts further with solvated electrons into $[Ca_n(OEt)_i(OH)_j(O)_k(I)_l]$, that is,

$$[Ca_N(OEt)_I(I)_L]^+ \xrightarrow{e_s} [Ca_n(OEt)_i(OH)_j(O)_k(I)_l]^+. \quad (26)$$

The processes of the cluster-ion formation are summarized in Scheme 4.

3. Dynamics of Reactions Following IR Multiphoton Excitation of Solvent Molecules

Multiphoton excitation of solvent molecules in a solution raises them in a metastable state, as if "hot" solvent molecules surround "cold" solute molecules. The metastable liquid is a peculiar medium in which superthermal reactions are expected to take place. In this section, we describe such a metastable liquid and explain ejection of molecules and clusters from a liquid beam whose solvent molecules are heated selectively by multiphoton excitation, while the remaining solute molecules stay cool.

3.1 Ejection Mechanisms of Molecules and Clusters.[62–67] As described, IR-multiphoton excitation of the solvent molecules in a liquid beam results in isolation of solute molecules in the gas phase. The solute molecules thus isolated are ionized by a UV laser for mass analysis. In this section, we describe the isolation mechanism of the solute molecules and clusters by the IR laser irradiation.

3.1.1 Isolation of Molecules and Clusters by IR-Multiphoton Excitation: Molecules and clusters are isolated in the gas phase by irradiation of an IR laser onto a liquid beam of a solution, and subsequently ionized by a UV laser illuminating outside the liquid beam for mass analysis. Let us exemplify IR-multiphoton excitation of an aqueous solution of resorcinol, $C_6H_4(OH)_2$, in the form of a liquid beam. The resorcinol molecule which acts as an ionization chromophore has a sufficiently low vapor pressure that the number density of the resorcinol molecule is very small in the gas phase. A

0.2-M resorcinol solution in water is irradiated with an IR laser (1.9 μm). The wavelength of the IR laser is resonant with the wavelength (1.9 μm) of the combination mode related to the OH stretching and the HOH bending vibrations of a solvent water molecule. A UV laser (266 nm) is focused at the distance of 0.4 mm outside the liquid beam with different delay times from the IR-laser irradiation, and the product photoions are mass-analyzed. Figure 12 shows typical mass spectra of ions produced from the liquid beam of a 0.2-M resorcinol solution in water at several different IR–UV delay times. Peaks in the mass spectra are assigned to hydrated resorcinol cluster ions, $C_6H_4(OH)_2^+ \cdot (H_2O)_n$. These mass spectra demonstrate that both the intensity and the size distributions of $C_6H_4(OH)_2^+ \cdot (H_2O)_n$ change significantly with the delay time. Figure 13 shows the intensity of $C_6H_4(OH)_2^+$ and the total intensity of all the cluster ions, $C_6H_4(OH)_2^+ \cdot (H_2O)_n$ ($n \geq 1$) as a function of the IR–UV delay time. In a delay time shorter than 3 μs (early-time domain), both the bare resorcinol ion, $C_6H_4(OH)_2^+$, and the cluster ions, $C_6H_4(OH)_2^+ \cdot (H_2O)_n$ are observed, but in the delay times longer than 3 μs (late-time domain), only the bare resorcinol ion is observed. The early- and late-time domains are attributed to the ejected species having high and low velocities, respectively, and hence the species produced in the early- and the late-time domains are, hereafter, named as the fast and the slow components, respectively. The appearance of the fast and the slow components indicates the presence of two different ejection processes: production of solvated clusters, $C_6H_4(OH)_2 \cdot (H_2O)_n$, with a hyperthermal velocity and production of bare resorcinol molecules, $C_6H_4(OH)_2$, with a thermal velocity.

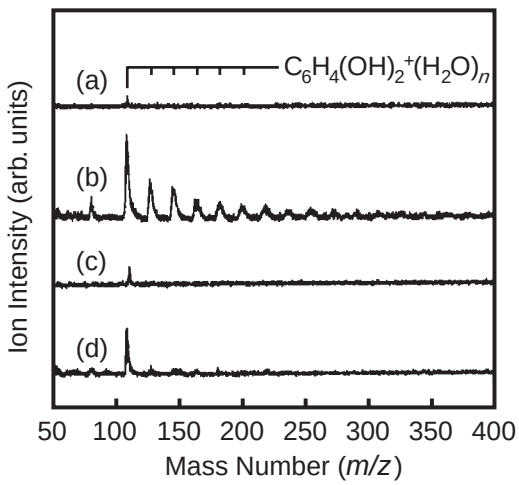

Fig. 12. Mass spectra of ions produced from the liquid beam of a 0.2-M resorcinol solution in water at the IR–UV delay times of (a) 0, (b) 0.3, (c) 3, and (d) 10 μs.

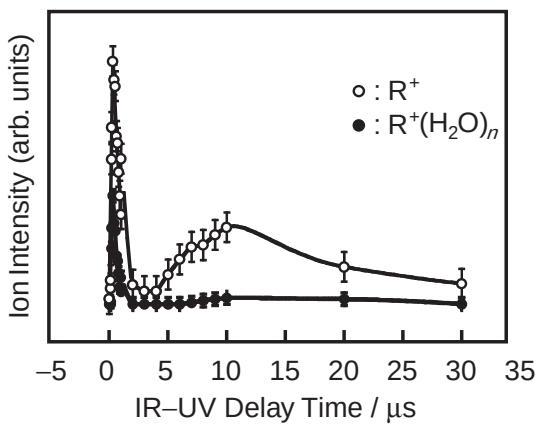

Fig. 13. The intensity of $C_6H_4(OH)_2^+$ (○) and the total intensity of all the cluster ions, $C_6H_4(OH)_2^+ \cdot (H_2O)_n$ ($n \geq 1$) (●) as a function of the IR–UV delay time.

Neutral clusters composed of resorcinol and water molecules are isolated through selective vibrational excitation of water molecules by the IR-laser irradiation, and are ionized by the UV laser. Several solvent water molecules may evaporate in the course of the IR-laser isolation and the UV-laser ionization to release some excess energy of the cluster as

$$C_6H_4(OH)_2(\text{soln}) + h\nu_{IR} \rightarrow C_6H_4(OH)_2 \cdot (H_2O)_N(\text{g}), \quad (27)$$

$$C_6H_4(OH)_2 \cdot (H_2O)_N(\text{g}) \rightarrow C_6H_4(OH)_2 \cdot (H_2O)_m(\text{g}) + (N-m)H_2O, \quad (28)$$

$$C_6H_4(OH)_2 \cdot (H_2O)_m(\text{g}) + 2h\nu_{UV} \rightarrow C_6H_4(OH)_2^+ \cdot (H_2O)_n(\text{g}) + (m-n)H_2O, \quad (29)$$

where (soln) and (g) represent species in the solution and in the gas phase, respectively. As shown in Fig. 13, the fast and the slow components consist of hydrated clusters and bare molecules, respectively. This finding indicates that the fast component has a lower internal energy than the slow component. We conclude that the fast and the slow components are produced via non-thermal and thermal processes, respectively. Upon the IR-laser irradiation, the solvated clusters are peeled off from the liquid-beam surface before establishment of a thermal equilibrium (fast component), while the bare molecules evaporate from the liquid beam after the excitation energy is thermalized (slow component).

3.1.2 Velocity Analysis of Fast Component: Let us examine the mechanism of the non-thermal ejection process by a detailed analysis of the fast component of hydrated phenol clusters which are ejected from a liquid beam of an aqueous solution of phenol under irradiation of an IR laser resonant to the OH stretch vibrational mode of liquid water. Here, the phenol molecule is the ionization chromophore. The clusters in the gas phase with a velocity distribution are distributed spatially when a UV probe-laser is fired for ionization of the clusters with a given IR–UV delay time, where the UV laser is placed on the same plane on which the IR laser is mounted. At the first place, the spatial distribution is measured while changing the distance, x, between the UV laser and the liquid beam. The ionized clusters in a small volume whose center is located at a distance of x away from the liquid beam are admitted into the mass spectrometer and detected as the intensity of I. If the clusters are isotropically distributed around the liquid beam, the total amount of clusters at the distance, x is proportional to $2\pi xI$.

In practice, the liquid beam is ablated by an IR laser (2.85 μm, 1 mJ/pulse) and the product neutral species are ionized when illuminated by a UV laser (270 nm, 0.1 mJ/pulse) while changing the distance, x. The hydrated phenol cluster ions, $Phe^+ \cdot (H_2O)_n$ ($0 \leq n \leq 30$), are detected by mass spectrosco-

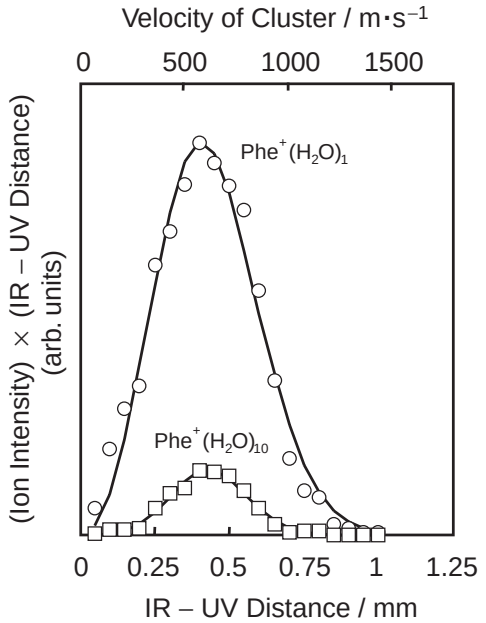

Fig. 14. Spatial distributions of $Phe^+ \cdot (H_2O)_1$ and $Phe^+ \cdot (H_2O)_{10}$, where an IR laser is irradiated at 0.7 μs before a UV laser is irradiated. The ordinate represents the product of the ion intensity and the IR–UV distance, which is proportional to a total amount of the product cluster ion at a distance away from the liquid beam, on the assumption that the product cluster ion distributes isotropically around the liquid beam.

py. Figure 14 shows the spatial distribution of $Phe^+ \cdot (H_2O)_1$ and $Phe^+ \cdot (H_2O)_{10}$ at the IR–UV delay time of 0.7 μs. The ordinate represents the product of the ion intensity, I, and the IR–UV distance, x. The spatial distributions thus obtained are fitted by using a conventional function, g, which is expressed as

$$g(x) = cx^2 \exp(-a(x-b)^2), \tag{30}$$

where a, b, and c are the fitting parameters employed (see solid best-fit curves in Fig. 14). Figure 15 shows the spatial distribution of the product cluster ions, $Phe^+ \cdot (H_2O)_n$ and its time evolution after the IR laser is fired; the data points are not shown to avoid congestion in the graphs. As shown in Fig. 15, the product cluster ions tend to distribute more widely in space at a longer elapsed time. In addition, the smaller cluster ions tend to distribute farther from the liquid beam.

The abundance of a product cluster ion at a given time is obtained by integrating $g(x)$ with respect to x. Figure 16 shows the abundance of the product cluster ion as a function of the mass number of the cluster at different delay times between the timings of firing the IR and the UV lasers. The abundances of the product cluster ions are normalized by that of $Phe^+ \cdot (H_2O)_1$. The result shows that the abundance, A, of the product cluster ion decreases almost exponentially with increase in the mass of the product cluster ion as

$$A(m) = A_0 e^{-\lambda m}, \tag{31}$$

where m is the mass of the product cluster ion, λ is the exponent, and A_0 is a parameter. The exponent, λ, increases with increase in the elapsed time. The exponent is obtained to be

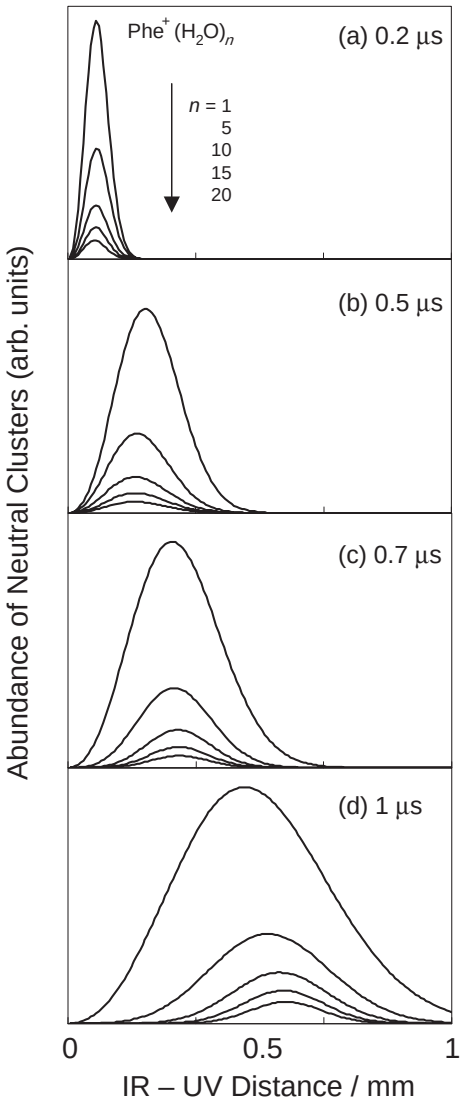

Fig. 15. Spatial distributions of $Phe^+ \cdot (H_2O)_n$ (n = 1, 5, 10, 15, and 20) and their time evolutions after the IR laser is fired; actual data points are not shown. The solid curves represent the best-fit results by using Eq. 1 (see text). The elapsed time from the IR-laser irradiation is set to be (a) 0.2, (b) 0.5, (c) 0.7, and (d) 1 μs.

0.00061 amu^{-1} at the time origin by extrapolation: the size distribution of the nascent clusters thus obtained is shown as a dotted line in Fig. 16.

A nascent cluster, $Phe \cdot (H_2O)_N$, is ejected while equilibrated with the surrounding liquid medium. It follows that $Phe \cdot (H_2O)_N$ has a Maxwellian velocity distribution:

$$f(u) = N_0 u^2 \exp\left(-\frac{m(u-V)^2}{2kT}\right), \tag{32}$$

where u, V, T, and m represent the velocity, the floating velocity, the translational temperature, and the mass of $Phe \cdot (H_2O)_N$, respectively, and N_0 is a constant for the normalization ($\int_0^\infty f(u)du = 1$). The spatial distributions shown in Fig. 15 are summed up and analyzed by the sum of the velocity distributions, F, of the nascent clusters as

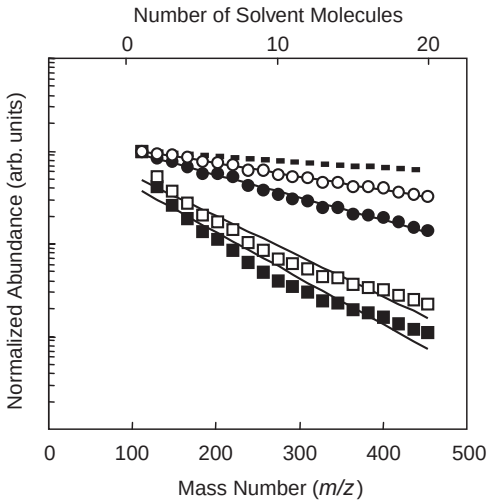

Fig. 16. Size distributions of the clusters produced at different elapsed times after an IR laser is fired. The elapsed times after the IR-laser irradiation are 0.2 (○), 0.5 (●), 0.7 (□), and 1 (■) μs. The abundances of the clusters are normalized so that the abundance of $Phe^{+}\cdot(H_2O)_1$ is unity. The abundance of the cluster given decreases exponentially with increase in the mass of the cluster. The dotted line represents the size distribution of the nascent clusters at the time origin estimated by extrapolation.

$$F(u) = \sum_{m=0}^{\infty} A_I(m) N_0(m) u^2 \exp\left(-\frac{m(u-V)^2}{2kT}\right), \qquad (33)$$

where $A_I(m)$ is the abundance of the nascent cluster, $Phe\cdot(H_2O)_N$, with its mass, m, which is given by Eq. 31 by substituting λ of 0.00061 amu^{-1}. The analysis gives the parameters, V and T, as a function of the IR–UV delay time as shown in Figs. 17a and 17b, respectively. As the IR–UV delay time increases, the floating velocity, V, increases from ~300 m/s to ~600 m/s, whereas the translational temperature, T, remains at ~6000 K. If the energy of the IR laser is fully converted to the internal energy of the liquid, the liquid beam is heated up to a temperature of ~500 K. The higher translational temperature (~6000 K) of the product clusters implies that the clusters can be regarded as the fast component and originate from a locally excited surface region of the liquid beam. It seems that the product clusters linger on the liquid-beam surface for several microseconds and hence the floating velocity of the product clusters increase with an increase in the IR–UV delay time.

In summary, we analyze the velocity distributions of the nascent hydrated phenol clusters, $Phe\cdot(H_2O)_N$, which are produced by irradiation of an IR laser onto a liquid beam of an aqueous solution of phenol. Results reveal that (1) the product clusters originate from a locally excited surface region of the liquid beam and (2) the product clusters linger for several microseconds on the liquid-beam surface.

3.1.3 Time Evolution of Cluster Ejection: Clusters are ejected into the gas phase at a delay time after firing an IR laser. This phenomenon is closely related to how the clusters are ejected from a liquid surface by the laser irradiation and hence the ejection mechanism can be investigated by analyzing this phenomenon. In this subsection, we describe the mechanism of the cluster ejection by using a liquid beam of an aqueous solution of aniline which an intense IR laser illuminates.

A liquid beam of a 0.2-M aqueous solution of aniline is crossed with a pulsed IR laser (2.96 μm). Neutral clusters ejected from the liquid beam under the IR laser irradiation are collimated by a 3-mm aperture placed at 25 mm away from the liquid beam, and are detected by a Daly multiplier mounted 1.65 m away from the liquid beam. In order to observe the time evolution of the clusters, a UV laser is illuminated at 0.4 mm outside the liquid beam so as to ionize the neutral species isolated by the IR laser. The aniline molecule is added as a chromophore of the UV-laser ionization. The ions produced by the UV-laser ionization are detected by the Daly multiplier without accelerating by an electric field, where the ions and the neutral species are detected in the same spectrum. Figure 18g shows a flight-time distribution of the neutral clusters produced from the 0.2-M aqueous solution of aniline under irradiation of the IR laser alone. Additionally, Figs. 18a–f show flight-time distributions of ions produced under irradiation of both the IR and the UV lasers (panels a–f) at different delay times (0.3–1.5 μs) between the timings of the IR and the UV laser irradiation, where no electric field is applied in the accel-

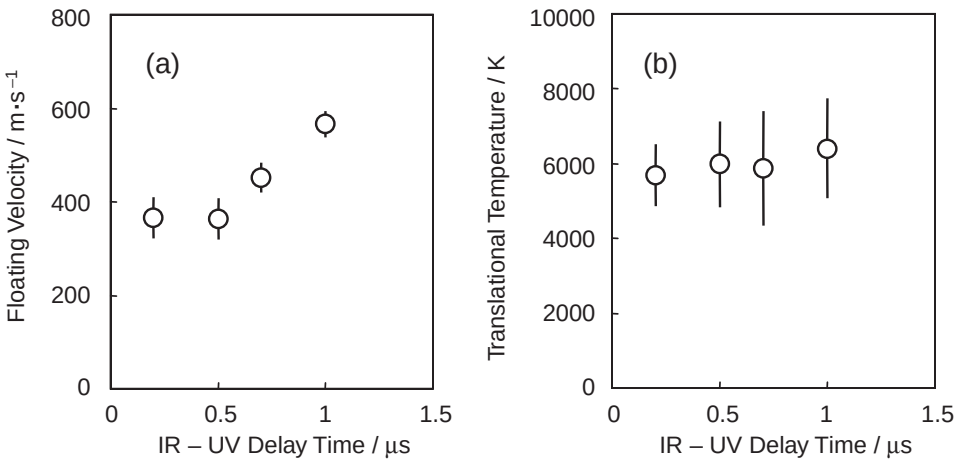

Fig. 17. (a) Floating velocity and (b) translational temperature of the clusters produced, as a function of the IR–UV delay time.

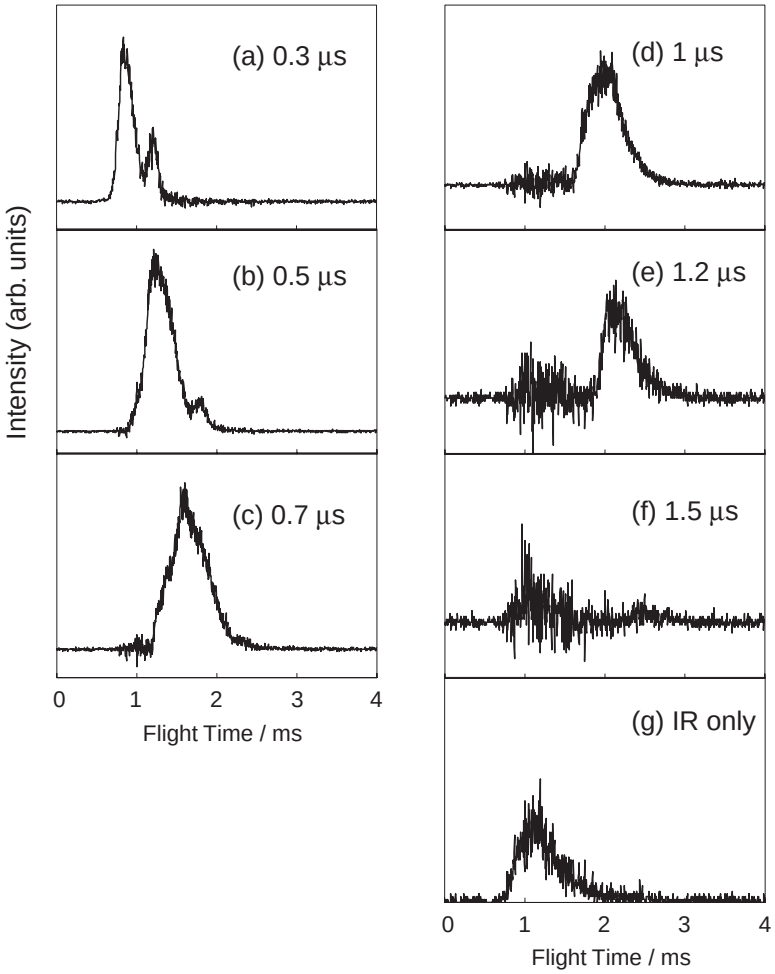

Fig. 18. Flight-time distributions obtained (a–f) under irradiation of the IR laser and a UV laser and (g) under irradiation of an IR laser only on the liquid beam of a 0.2-M aqueous solution of aniline. The IR and the UV lasers are focused onto the liquid beam and at 0.5 mm away from the liquid beam, respectively. The delay times between the timings of firing the IR to the UV lasers are (a) 0.3, (b) 0.5, (c) 0.7, (d) 1, (e) 1.2, and (f) 1.5 μs.

eration region. The flight-time distribution obtained by irradiation of the IR laser alone (panel g) is subtracted from those obtained by irradiation of both the IR and UV lasers, as shown in panels a–f. Namely, flight-time distributions a–f are given by the ions produced by irradiation of the UV laser. The cluster ions travel in the gas phase with the same velocity before the ionization, because no electric field is applied in the ionization region. The flight-time distributions exhibit an intense peak in addition to a small side peak (panels a and b). The flight time increases with increase in the IR–UV delay time.

Under irradiation of an intense IR-laser pulse on a liquid-beam surface, various chemical species are ejected from the surface due to the ablation by the laser pulse at a delay time after the laser pulse is fired. This delay time is interpreted as a "start time", during which the number density of bubbles formed in a superheated portion of the liquid beam increases up to a critical value. When the number of such bubbles reaches the critical value, the superheated portion explodes into pieces (clusters). Figure 19 shows the procedure of obtaining the start time of the photoionized clusters, t_s, where x and t represent the spatial position (the distance from the liquid beam) and the time elapsed after the IR laser is fired, respectively, x_i represents the spatial position at which the UV ionization laser is fired at the time t_i, and x_d represents the position of the detector at which a product arrives at the time t_d. Let us suppose that a cluster is ejected from a liquid beam by an IR-

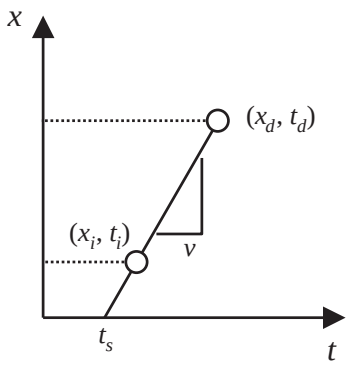

Fig. 19. Schematic drawing which explains the procedure for obtaining the start time at which clusters are ejected from a liquid beam; the time origin of the start time is the time of a laser pulsing.

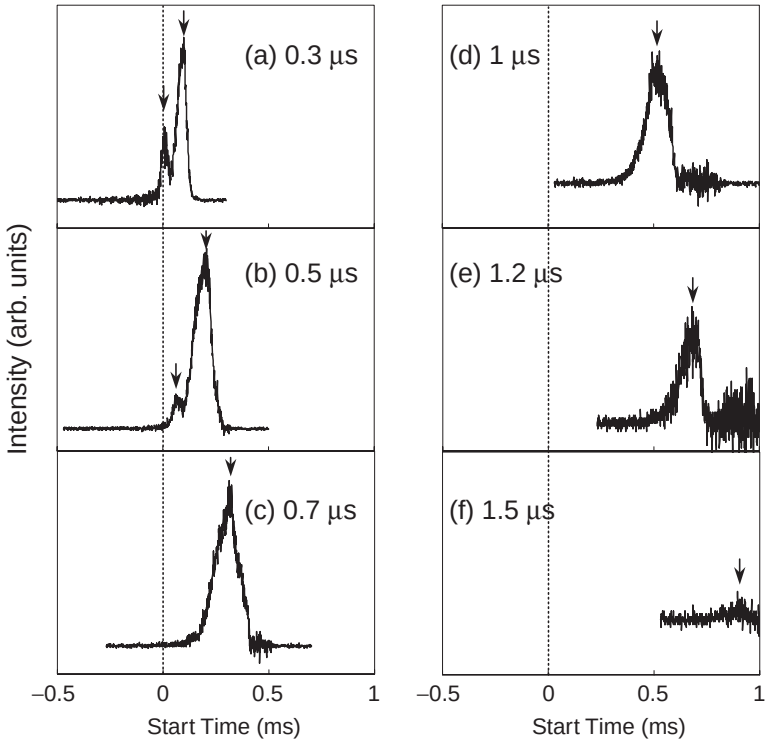

Fig. 20. Start-time distributions of photoionized clusters calculated from the flight-time distributions (see Fig. 18). A 0.2-M aqueous solution of aniline is employed. The panels designated by a, b, c, ... correspond to those designated by a, b, c, ... given in Fig. 18.

laser pulse. The position, x, is expressed in terms of t as

$$x = v(t - t_s), \tag{34}$$

where v represents the velocity of the cluster. The values of v and t_s are obtained from the given values of (x_i, t_i) and (x_d, t_d). With $x_d = 1.65$ m, one obtains the start-time distribution and the velocity distribution of the photoionized clusters from the flight-time distribution (see Fig. 18), as shown in Figs. 20 and 21, respectively. The start-time distribution consists of a small peak at $t_s \sim 0$ μs and a large peak at $0.1 \leq t_s \leq 1$ μs (see panels a and b of Fig. 20, for instance). The small peak appearing at $t_s \sim 0$ μs is assignable to clusters ejected from the surface because no appreciable time is available for the clusters to be liberated from the liquid beam. On the other hand, the large peak is attributed to clusters from the inside of the beam because they need a substantial time ($t_s \leq 1$ μs) to be released from the liquid beam; the clusters linger on the surface for a while before they are completely liberated into the gas phase, due to collisions with a dense cloud of water vapor in their vicinity. The lingering of the clusters is manifested on the v–t_s relationship depicted in Fig. 22, as supported by the decrease of the cluster velocity with t_s. We conclude that the clusters from the surface and from the inside of the liquid beam correspond to the clusters of the fast and the slow components, respectively, because the velocity of the clusters decreases during the lingering process.

In summary, the start-time distribution of the neutral clusters produced by irradiating an IR laser onto the liquid beam is derived from the flight-time distributions of ions produced by the UV laser irradiation. We conclude that the clusters are produced from the surface and from the inside of the liquid beam. The cluster ejection is likely to proceed via inhomogeneous local heating followed by explosion of the liquid beam.

3.2 Reaction Dynamics of Molecules and Clusters Ejected from Liquid Beam.[68,69] Irradiation of an IR laser onto a liquid beam causes molecules and clusters in the liquid beam to be isolated in the gas phase. The isolation dynamics is explained in this section by using studies on molecules ejected from a liquid beam of aqueous solutions: multiphoton ionization of adenine molecules and a photoionization-induced nucleation in the vicinity of phenol molecules.

3.2.1 Multiphoton Ionization of Adenine Salts: Biological molecules work only properly in an aqueous solution in cooperation with its solvent water molecules. Roles of water molecules on the biological function could be elucidated by studying functions of a target molecule isolated and hydrated. To begin with, adenine salts (adenine di-hydrochloride and sodium adeninate) are isolated from a liquid beam of aqueous acidic and alkaline solutions of adenine by irradiation of an IR laser. The isolated adenine salts are ionized by a UV laser in the gas phase.

Figure 23 shows a typical mass spectrum of ions produced from a 0.1-M aqueous solution of adenine di-hydrochloride, A·2HCl, under irradiation of an IR laser (3 μm) with subsequent irradiation of a UV laser (270 nm) at 2 μs after the IR laser firing. The IR laser is focused onto the liquid beam of an aqueous solution of adenine, whereas the UV laser is focused at a position 0.5 mm away from the liquid beam. Peaks in the mass spectrum are assigned to a protonated adenine ion, its hydrated cluster ions, $AH^+ \cdot (H_2O)_n$ ($n = 0$–5), and proto-

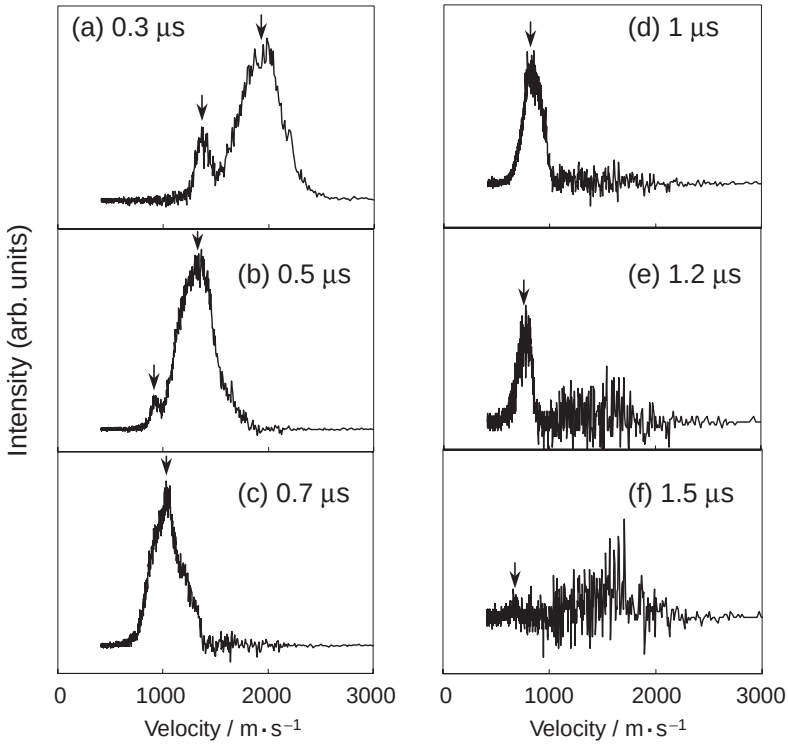

Fig. 21. Velocity distributions of the photoionized clusters calculated from the flight-time distributions given in Fig. 18. The sample solution employed is a 0.2-M aqueous solution of aniline. The panels designated by a, b, c, ... correspond to those designated by a, b, c, ... given in Figs. 18 and 20.

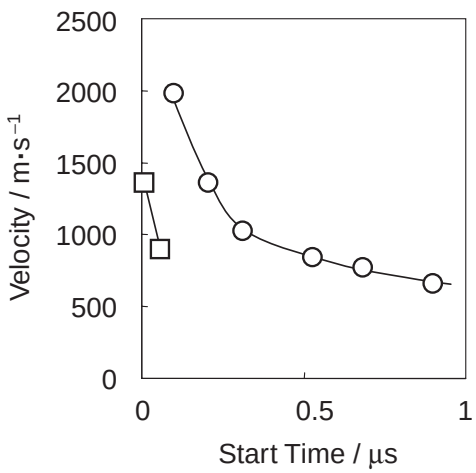

Fig. 22. Velocities of the fast and the slow components in the flight-time distribution as a function of the start time, which are obtained from the corresponding peak positions of the start time and the velocity shown in Figs. 19 and 20, respectively. The solid curves are eye guides.

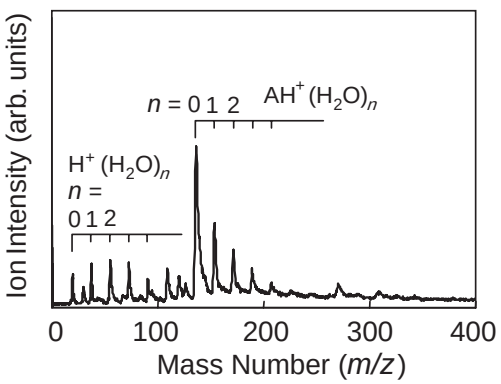

Fig. 23. Mass spectrum of ions produced from a 0.1-M aqueous solution of adenine di-hydrochloride, A·2HCl, under irradiation of an IR laser (3 μm) with subsequent irradiation of a UV laser (270 nm) at 2 μs after the IR laser is fired. The IR laser is focused onto the liquid beam, whereas the UV laser is focused at 0.5 mm away from the liquid beam.

nated water clusters, $H^+\cdot(H_2O)_n$ ($n = 0$–5). In order to confirm the mass assignment mentioned above, heavy water (D_2O) is used instead of H_2O as a solvent.

The intensities of all the ions observed are measured at different concentrations of A·2HCl. Figure 24 shows the intensities of $AH^+\cdot(H_2O)_1$ and $H^+\cdot(H_2O)_1$ as a function of the intensity of AH^+ measured by changing the concentration of A·2HCl. The abscissa is a measure which is proportional to the concentration of A·2HCl. The I_{X^+} vs I_{AH^+} relationships for $AH^+\cdot(H_2O)_1$ and $H^+\cdot(H_2O)_1$ are given by the relation

$$I_{X^+} = BI_{AH^+}{}^b, \tag{35}$$

where I_{X^+} represents the intensity of X^+ ($X^+ = AH^+\cdot(H_2O)_1$ and $H^+\cdot(H_2O)_1$), b represents the number of A·2HCl molecules involved in the production of X^+ on the assumption that one A·2HCl is involved in the production of one AH^+, and B is a constant. The best-fit values of b turn out to be 1.03 and 1.37 for $AH^+\cdot(H_2O)_1$ and $H^+\cdot(H_2O)_1$, respectively.

As an adenine molecule has basic nitrogen atoms, the mole-

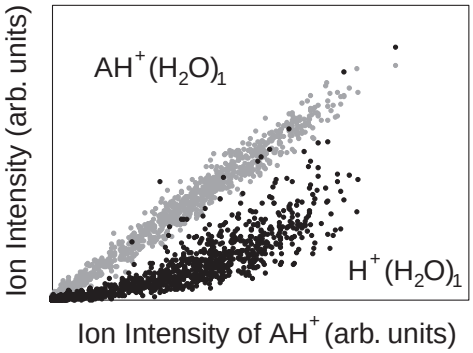

Fig. 24. Intensities of $AH^+ \cdot (H_2O)_1$ and $H^+ \cdot (H_2O)_1$ as a function of the intensity of AH^+ measured simultaneously.

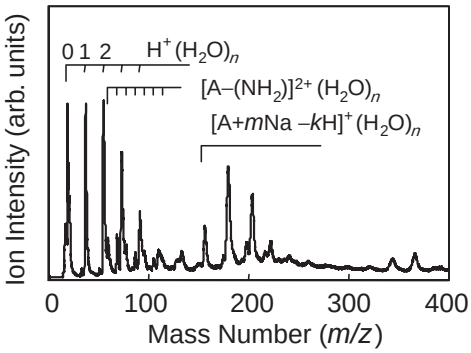

Fig. 25. Mass spectrum of ions produced from a liquid beam of a 0.1-M adenine containing $(0.1 + \alpha)$-M sodium hydroxide in water by irradiation of an IR laser (3 μm) and a UV laser (270 nm) with the delay time of 2 μs.

cule is dissolved in a HCl solution as a protonated form: $AH_2^{2+} \cdot 2Cl^-$ in an aqueous solution of 0.1-M adenine and 0.2-M HCl. In fact, the solubility of adenine is less than 0.1 M either in pure water or in an aqueous HCl solution of less than 0.2 M. The neutral species produced by the IR laser irradiation is assigned to $AH_2^{2+} \cdot 2Cl^-$, because: (1) the ionic components, AH_2^{2+} and $2Cl^-$, are initially present in the HCl solution; (2) hydrochloric acid is needed to dissolve adenine into water; and (3) the species is neutral. Photoionization of the neutral species, $AH_2^{2+} \cdot 2Cl^-$, by the UV laser gives AH^+, H^+, and their hydrated clusters. The ion, AH^+, is produced by a four-photon ionization of $AH_2^{2+} \cdot 2Cl^-$ in the gas phase, as revealed by a UV-laser power dependence.

The hydrated cluster ion, $AH^+ \cdot (H_2O)_1$, is produced by association of H_2O with AH^+ thus produced via the above processes; the $AH^+ \cdot (H_2O)_1$ intensity increases proportionally with increase in the AH^+ intensity (see Fig. 24). In contrast, $H^+ \cdot (H_2O)_n$ is produced mainly by collisional proton transfer from AH^+ to $(H_2O)_{n'}$

$$AH^+ + (H_2O)_{n'} \rightarrow A + H^+ \cdot (H_2O)_n + (n' - n)H_2O, \quad (36)$$

because the $H^+ \cdot (H_2O)_n$ intensity is nearly proportional to the AH^+ intensity; in reality, the intensity of $H^+ \cdot (H_2O)_n$ is found to be proportional to the AH^+ intensity to the power of 1.37. Such deviation from linearity is ascribable to the operation of an additional process to the production of $H^+ \cdot (H_2O)_n$ where one more $AH_2^{2+} \cdot 2Cl^-$ is involved in generating $H^+ \cdot (H_2O)_n$. The most likely process is

$$AH^+ + AH_2^{2+} \cdot 2Cl^- \rightarrow [A_2H_3^{3+} \cdot 2Cl^-], \quad (37)$$

$$[A_2H_3^{3+} \cdot 2Cl^-] + (H_2O)_{n'} \rightarrow [A_2H_2^{2+} \cdot 2Cl^-] + H^+ \cdot (H_2O)_n + (n' - n)H_2O. \quad (38)$$

Figure 25 shows a typical mass spectrum of ions produced from the liquid beam of a 0.1-M adenine containing $(0.1 + \alpha)$-M sodium hydroxide in H_2O by irradiation of an IR laser (3 μm) and a UV laser (270 nm) with a delay time of 2 μs. Peaks in the mass spectrum are assigned as $H^+ \cdot (H_2O)_n$ $(n = 0–5)$ and $[A + m\text{Na-}k\text{H}]^+ \cdot (H_2O)_n$ $((m, k) = (1, 2), (2, 2), (2, 3)$, and $(3, 3))$. In addition, doubly charged ions, $[A\text{-}N\text{-}H]^{2+} \cdot (H_2O)_n$, are observed in the mass spectrum. Note that the quantity inside of the brackets, [ ], represents the molecular formula of the ion and the subsequent superscript of that represents the charge of the ion.

In an aqueous alkaline solution of adenine, adenine is present in a form of $[A\text{-}H]^-$ at pK_a of 4.07, $[A\text{-}2H]^{2-}$ at pK_a of 9.67 and could be $[A\text{-}3H]^{3-}$ at a higher value of pK_a. All the species, $[A\text{-}i\text{H}]^{i-} \cdot i\text{Na}^+$ $(i = 1–3)$, present in the solution containing 0.1 M of NaOH are likely to be isolated by the IR laser irradiation. These neutral species thus isolated are photoionized by the UV laser into $H^+ \cdot (H_2O)_n$ $(n = 0–5)$ and singly charged ions, $[A + m\text{Na-}k\text{H}]^+ \cdot (H_2O)_n$ $((m, k) = (1, 2), (2, 2), (2, 3)$, and $(3, 3))$ probably through doubly charged ions, $[[A\text{-}i\text{H}]^{i-} \cdot i\text{Na}^+]^{2+}$ $(i = 1–3)$. The involvement of these doubly charged ions in the ionization is rationalized because 1) doubly charged ions, $[A\text{-}N\text{-}H]^{2+} \cdot (H_2O)_n$, are produced in the photoionization (see Fig. 25), and 2) the reaction intermediates postulated are produced directly by abstraction of two electrons from the species isolated from the liquid beam by the IR laser irradiation. The photoionization processes involving $[A\text{-}H]^-\text{Na}^+$ $(i = 1)$ are expressed as follows:

$$[A\text{-}H]^- \cdot \text{Na}^+ + nh\nu \rightarrow [A\text{-}H] \cdot \text{Na}^+, \quad (39)$$

$$[A\text{-}H] \cdot \text{Na}^+ + n'h\nu \rightarrow [A\text{-}H]^+ \cdot \text{Na}^+, \quad (40)$$

$$[A\text{-}H]^+ \cdot \text{Na}^+ \rightarrow [A\text{-}N\text{-}H]^{2+} \quad \text{(decomposition)}, \quad (41)$$

$$[A\text{-}H]^+ \cdot \text{Na}^+ + (H_2O)_n \rightarrow [A\text{-}2H] \cdot \text{Na}^+ + H^+ \cdot (H_2O)_n \quad \text{(proton transfer)}. \quad (42)$$

Although the structure of $[A\text{-}N\text{-}H]^{2+}$ is unknown, it is plausible that the primary amino group in $[A\text{-}H]^+ \cdot \text{Na}^+$ is replaced to a hydrogen atom; the replacement reaction is driven by Coulomb repulsion within the doubly charged ion, $[A\text{-}H]^+ \cdot \text{Na}^+$. Photoionization of $[[A\text{-}i\text{H}]^{i-} \cdot i\text{Na}^+]^{2+}$ $(i = 2, 3)$ is expressed in a similar manner.

3.2.2 Ionization-Induced Nucleation: IR-laser ablation of a liquid beam of a solution produces a dense cloud of solute and solvent molecules in the vicinity of the liquid beam. In this section, we describe nucleation initiated by phenol ions in a cloud of water molecules produced by IR laser irradiation on a liquid beam of an aqueous solution of phenol.

Figure 26 shows typical mass spectra of ions produced by irradiation of a pulsed IR (3 μm, 2 mJ/pulse) and UV (270 nm, 0.05 mJ/pulse) lasers with a delay time of 1 μs. The IR laser is focused on the liquid beam of a 0.2-M aqueous solution of phenol, whereas the UV laser is focused at a location 0.5 mm away from the liquid beam. Peaks in the mass spectrum are assigned to hydrated phenol cluster ions, $Phe^+ \cdot (H_2O)_n$ $(n = 0–20)$. The ions are accelerated by a pulsed electric field

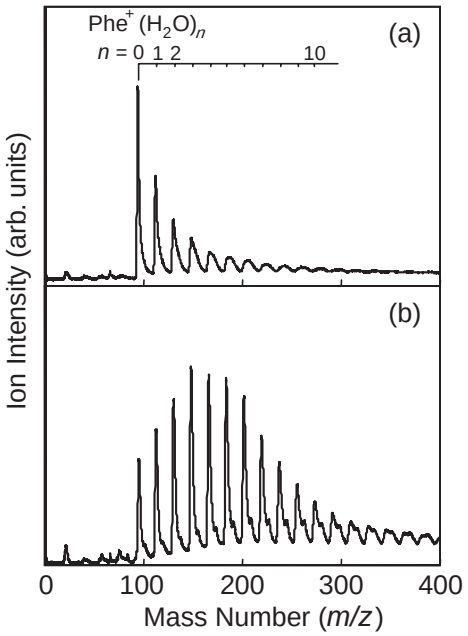

Fig. 26. Mass spectra of ions produced by irradiation of an IR laser (3 μm) and a pulsed UV laser (270 nm) with a delay time of 1 μs. The IR laser is focused on the liquid beam of a 0.2-M aqueous solution of phenol, while the UV laser is focused at 0.5 mm away from the liquid beam. The peaks in the mass spectrum are assigned to hydrated phenol cluster ions, $Phe^+ \cdot (H_2O)_n$ ($n = 0$–20). The residence times are set to (a) 0 and (b) 1 μs.

with a delay time from the UV laser, which is denoted as "residence time" hereafter. The spectra shown in panels a and b of Fig. 26 are those with the residence times of 0 and 1 μs, respectively; a bare solute ion, Phe^+, is most abundant and hydrated cluster ions, $Phe^+ \cdot (H_2O)_n$, have decreasing intensities with increasing size n with the residence time of 0 μs (see panel a), while $Phe^+ \cdot (H_2O)_n$, are more abundant than Phe^+ with the residence time of 1 μs (see panel b).

The IR laser irradiation onto the liquid beam produces a dense cloud of phenol and water molecules in the vicinity of the liquid beam. The phenol molecule in the cloud is selectively ionized by the ionization UV laser. The phenol ions grow into hydrated phenol cluster ions by collecting water molecules in the dense cloud of water vapor (see panel b of Fig. 26). Ejection of phenol molecules and growth of its ion are expressed as

$$H_2O(soln) + nh\nu_{IR} \rightarrow Phe(g) + H_2O(g), \quad (43)$$

$$Phe(g) + 2h\nu_{UV} \rightarrow Phe^+(g), \quad (44)$$

$$Phe^+(g) + H_2O(g) \rightarrow Phe^+ \cdot (H_2O)_1(g), \quad (45)$$

$$Phe^+ \cdot (H_2O)_1(g) + H_2O(g) \rightarrow Phe^+ \cdot (H_2O)_2(g), \quad (46)$$

$$\cdots,$$

where (soln) and (g) represent species in solution and gas phases, respectively.

The density of the cloud of water molecules as a function of the residence time is estimated by considering the growth process of bare phenol ion, Phe^+, into $Phe^+ \cdot (H_2O)_1$. As shown in process 45, bare phenol ions, Phe^+, are depleted during the residence time due to hydration. By regarding process 45 as a first-order reaction,[89] the decrement, $-\Delta[Phe^+]$, by a short time interval, Δt, is proportional to the number density of water molecules around a given phenol ions as

$$-\Delta[Phe^+] = k[H_2O][Phe^+]\Delta t, \quad (47)$$

where [X] and k represent the number density of X and the rate constant, respectively. The relative intensity, I_P, of Phe^+ is proportional to the number density of Phe^+ as

$$I_P = c[Phe^+], \quad (48)$$

where c is a proportionality constant. The value of $k[H_2O]$ is derived from Eqs. 47 and 48 as

$$k[H_2O] = -\frac{\Delta[Ph^+]}{\Delta t \cdot [Ph^+]} = -\frac{c\Delta I_P}{\Delta t \cdot cI_P} = -\frac{\Delta I_P}{\Delta t \cdot I_P}. \quad (49)$$

The number density of water molecules in the cloud is estimated from $k[H_2O]$ for a given k. In the system of Phe^+ and H_2O, a charge-induced dipole interaction is the strongest attractive force. Under the assumption that the charge-induced dipole interaction is dominant, the rate constant, k, is given by the Langevin rate constant:

$$k = \left(\frac{\alpha e^2}{4\varepsilon_0{}^2\mu}\right)^{\frac{1}{2}}, \quad (50)$$

where e, ε_0, α, and μ represent the elementary charge (1.602×10^{-19} C), the dielectric constant of a vacuum (8.854×10^{-12} F m^{-1}), the polarizability of water vapor (1.63×10^{-40} C^2 m^2 J^{-1}), and the reduced mass of a phenol–water collision pair, respectively. Using the k value thus calculated (7.3×10^{-16} m^3 molecule^{-1} s^{-1}), one obtains the number density of water molecules. Note that the k value is, in reality, smaller than that we employed in the analysis, because (1) the Langevin rate constant gives the upper limit and (2) the effective k value decreases if one takes a higher order reaction for process 45 into account.[89] Then, one obtains the lower limit of the number density of water molecules by this analysis. Figure 27 shows the number density of water molecules in the cloud as a function of the residence time. The number density is initially $\sim 10^{21}$ molecule m^{-3} and diminishes in a time scale of ~ 2 μs.

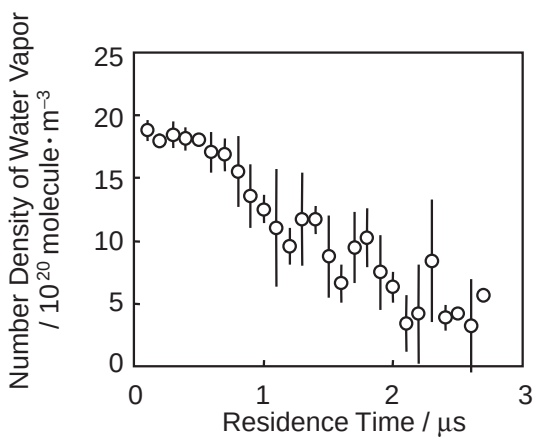

Fig. 27. Number density of water vapor in the vicinity of Phe^+ as a function of the residence time.

In summary, we have shown that an ionization induced nucleation proceeds in a cloud of molecules produced by irradiation of an IR laser onto a liquid beam. A kinetic model gives us the number density of the cloud as a function of the elapsed time after the IR laser irradiation.

4. Concluding Remarks

We have described reaction dynamics of molecules in solutions induced by multiphoton excitation by use of the liquid-beam technique combined with laser-excitation mass-spectrometry. Our results revealed that specific chemical reactions are initiated in the solutions by irradiation of a laser with an appropriate power and wavelength. The reaction mechanisms are elucidated by observing the reaction intermediates and the products isolated from the liquid beam into the gas phase. The findings in these studies will provide useful information for the synthetic studies on the multiphoton chemical reactions in solutions.

Our research projects on multiphoton chemical reactions in solutions were supported by the Special Cluster Research Project of Genesis Research Institute, Inc. We are grateful to the Institute for support and encouragement. We are grateful to Professor Takashi Nagata and Mr. Yoshihiro Takeda for their contributions in the early stages of the liquid-beam studies. We would thank especially Dr. Noriko Horimoto and Dr. Namiki Toyama for their contributions to the studies on IR multiphoton excitation of the liquid beam.

References

1 M. A. Miranda, J. P. Pérez-Prieto, E. Font-Sanchis, and J. C. Scaiano, *Acc. Chem. Res.*, **34**, 717 (2001).
2 M. A. Miranda, E. Font-Sanchis, J. P. Pérez-Prieto, and J. C. Scaiano, *J. Org. Chem.*, **64**, 7842 (1999).
3 J. T. Banks, H. Garcia, M. A. Miranda, J. P. Pérez-Prieto, and J. C. Scaiano, *J. Am. Chem. Soc.*, **117**, 5049 (1995).
4 J. C. Scaiano and J. T. Banks, *J. Braz. Chem. Soc.*, **6**, 199 (1995).
5 R. M. Wilson and K. A. Schnapp, *Chem. Rev.*, **93**, 223 (1993).
6 R. M. Wilson, K. A. Schnapp, K. Hannemann, D. M. Ho, H. R. Memarian, A. Azadnia, A. R. Pinhas, and T. M. Figley, *Spectrochim. Acta*, **46A**, 551 (1990).
7 R. Srinivasan and A. P. Ghosh, *Chem. Phys. Lett.*, **143**, 546 (1988).
8 J. Pola, M. Urbanová, Z. Bastl, Z, Plzák, J. Šubrt, V. Vorlíček, I. Gregora, C. Crowley, and R. Taylor, *Carbon*, **35**, 605 (1997).
9 R. Katoh, H. Yokoi, S. Usuba, Y. Kakudate, and S. Fujiwara, *Chem. Phys. Lett.*, **291**, 305 (1998).
10 J. J. Belbruno, G. Siuzdak, and S. North, *Chem. Phys. Lett.*, **166**, 167 (1990).
11 G. Siuzdak and J. J. Belbruno, *Laser Chem.*, **11**, 83 (1991).
12 G. Siuzdak, S. North, and J. J. Belbruno, *J. Phys. Chem.*, **95**, 5190 (1991).
13 J. J. Belbruno, G. Siuzdak, and S. North, *Laser Chem.*, **10**, 177 (1990).
14 J. T. Banks and J. C. Scaiano, *J. Am. Chem. Soc.*, **115**, 6409 (1993).
15 W. Adam and K. Schneider, *J. Chem. Soc., Perkin Trans., 2*, **1997**, 441.
16 W. Adam, K. Schneider, M. Stapper, and S. Steenken, *J. Am. Chem. Soc.*, **119**, 3280 (1997).
17 "Laser Ablation and Desorption," ed by J. C. Miller and R. F. Haglund, Jr., Academic Press, San Diego (1998).
18 K. Tanaka, H. Waki, Y. Ido, S. Akita, Y. Yoshida, and T. Yoshida, *Rapid Commum. Mass Spectrom.*, **2**, 151 (1988).
19 M. Karas, D. Bachmann, U. Bahr, and F. Hillenkamp, *Int. J. Mass Spectrom. Ion Processes*, **78**, 53 (1987).
20 M. Karas and F. Hillenkamp, *Anal. Chem.*, **60**, 2299 (1988).
21 W. Kleinekofort, J. Avdiev, and B. Brutschy, *Int. J. Mass Spectrom.*, **152**, 135 (1996).
22 W. Kleinekofort, M. Schweitzerm, J. W. Engels, and B. Brutschy, *Int. J. Mass Spectrom.*, **156**, 195 (1996).
23 W. Kleinekofort, M. Schweitzerm, J. W. Engels, and B. Brutschy, *Int. J. Mass Spectrom.*, **163**, 1 (1997).
24 F. Sobott, W. Kleinekofort, and B. Brutschy, *Anal. Chem.*, **69**, 3587 (1997).
25 F. Sobott, A. Wattenberg, H. Barth, and B. Brutschy, *Int. J. Mass Spectrom.*, **185**, 271 (1999).
26 A. Wattenberg, F. Sobott, and B. Brutschy, *Rapid Commum. Mass Spectrom.*, **14**, 859 (2000).
27 A. Wattenberg, F. Sobott, H. Barth, and B. Brutschy, *Int. J. Mass Spectrom.*, **203**, 49 (2000).
28 A. Charvat, E. Lugovoj, M. Faubel, and B. Abel, *Eur. Phys. J. D*, **20**, 573 (2002).
29 A. Charvat, E. Lugovoj, M. Faubel, and B. Abel, *Rev. Sci. Instrum.*, **75**, 1209 (2004).
30 H. Siegbahn, *J. Phys. Chem.*, **89**, 898 (1985).
31 H. Siegbahn and K. Siegbahn, *J. Electron Spectrosc. Relat. Phenom.*, **2**, 319 (1973).
32 R. E. Ballard, J. Jones, and D. Hart, *J. Electron Spectrosc. Relat. Phenom.*, **26**, 31 (1982).
33 H. Aulich, P. Delahay, and L. Nemec, *J. Chem. Phys.*, **59**, 2354 (1973).
34 I. Watanabe, J. B. Flanagan, and P. Delahay, *J. Chem. Phys.*, **73**, 2057 (1980).
35 H. Morgner, *Surf. Sci.*, **317**, 407 (1994).
36 M. E. Saecker, S. T. Govoni, D. V. Kowalski, and G. M. Nathanson, *Science*, **252**, 1421 (1991).
37 M. E. King, G. M. Nathanson, M. A. Hanning-Lee, and T. K. Minton, *Phys. Rev. Lett.*, **70**, 1026 (1993).
38 J. Klassen and G. M. Nathanson, *Science*, **273**, 333 (1997).
39 A. Furlan, *Chem. Phys. Lett.*, **275**, 239 (1997).
40 A. Furlan, *Chem. Phys. Lett.*, **309**, 157 (1999).
41 M. Faubel and Th. Kisters, *Nature*, **339**, 527 (1989).
42 M. Faubel, S. Schlemmer, and J. P. Toennies, *Z. Phys. D*, **10**, 269 (1988).
43 M. Faubel, B. Steiner, and J. P. Toennies, *J. Chem. Phys.*, **106**, 9013 (1997).
44 M. Faubel, B. Steiner, and J. P. Toennies, *Mol. Phys.*, **90**, 327 (1996).
45 B. Steiner, M. Faubel, and J. P. Toennies, *J. Electron Spectrosc. Relat. Phenom.*, **95**, 159 (1998).
46 M. Faubel, "Photoionization and Photodetachment," ed by C.-Y. Ng, World Scientific, Singapore (2000), pp. 634–690.
47 W. L. Holstein, L. J. Hayes, E. M. C. Robinson, G. S. Laurence, and M. A. Buntine, *J. Phys. Chem. B*, **103**, 3035 (1999).
48 W. L. Holstein, M. R. Hammer, G. F. Metha, and M. A. Buntine, *Int. J. Mass Spectrom.*, **207**, 1 (2001).
49 T. Kondow and F. Mafuné, *Annu. Rev. Phys. Chem.*, **51**,

731 (2000).
50 F. Mafuné, N. Horimoto, J. Kohno, and T. Kondow, "Progress in Experimental and Theoretical Studies of Clusters," ed by T. Kondow and F. Mafuné, World Scientific, Singapore (2003), pp. 261–276.
51 F. Mafuné, Y. Takeda, T. Nagata, and T. Kondow, *Chem. Phys. Lett.*, **199**, 615 (1992).
52 F. Mafuné, J. Kohno, T. Nagata, and T. Kondow, *Chem. Phys. Lett.*, **218**, 7 (1994).
53 F. Mafuné, J. Kohno, and T. Kondow, *J. Chin. Chem. Soc.*, **42**, 449 (1994).
54 J. Kohno, F. Mafuné, and T. Kondow, *J. Phys. Chem. A*, **104**, 243 (2000).
55 F. Mafuné, Y. Takeda, T. Nagata, and T. Kondow, *Chem. Phys. Lett.*, **218**, 234 (1994).
56 F. Mafuné, Y. Hashimoto, M. Hashimoto, and T. Kondow, *J. Phys. Chem.*, **99**, 13834 (1995).
57 F. Mafuné, Y. Hashimoto, and T. Kondow, *Chem. Phys. Lett.*, **274**, 127 (1997).
58 J. Kohno, F. Mafuné, and T. Kondow, *J. Am. Chem. Soc.*, **116**, 9801 (1994).
59 J. Kohno, N. Horimoto, F. Mafuné, and T. Kondow, *J. Phys. Chem.*, **99**, 15627 (1995).
60 F. Mafuné, J. Kohno, and T. Kondow, *J. Phys. Chem.*, **100**, 4476 (1996).
61 F. Mafuné, J. Kohno, and T. Kondow, *J. Phys. Chem.*, **100**, 10041 (1996).
62 N. Horimoto, F. Mafuné, and T. Kondow, *Chem. Lett.*, **1996**, 159.
63 N. Horimoto, F. Mafuné, and T. Kondow, *J. Phys. Chem.*, **100**, 10046 (1996).
64 Y. Hashimoto, F. Mafuné, and T. Kondow, *J. Phys. Chem.*, **102**, 4295 (1997).
65 N. Horimoto, F. Mafuné, and T. Kondow, *J. Phys. Chem. B*, **103**, 1900 (1999).
66 N. Horimoto, F. Mafuné, and T. Kondow, *J. Phys. Chem. B*, **103**, 9540 (1999).
67 H. Matsumura, F. Mafuné, and T. Kondow, *J. Phys. Chem.*, **99**, 5861 (1995).
68 J. Kohno, F. Mafuné, and T. Kondow, *J. Phys. Chem. A*, **103**, 1518 (1999).
69 J. Kohno, F. Mafuné, and T. Kondow, *J. Phys. Chem. A*, **104**, 1079 (2000).
70 J. Kohno, F. Mafuné, and T. Kondow, *J. Phys. Chem. A*, **105**, 5990 (2001).
71 N. Horimoto, J. Kohno, F. Mafuné, and T. Kondow, *J. Phys. Chem. A*, **103**, 9569 (1999).
72 N. Horimoto, J. Kohno, F. Mafuné, and T. Kondow, *Chem. Phys. Lett.*, **318**, 536 (2000).
73 J. Kohno, F. Mafuné, and T. Kondow, *J. Phys. Chem. A*, **105**, 8939 (2001).
74 J. Kohno, N. Toyama, F. Mafuné, and T. Kondow, *Isr. J. Chem.*, **44**, 215 (2004).
75 J. Kohno, F. Mafuné, and T. Kondow, *Chem. Lett.*, **2002**, 562.
76 J. Kohno, F. Mafuné, and T. Kondow, *J. Phys. Chem. A*, **108**, 971 (2004).
77 J. Kohno, F. Mafuné, and T. Kondow, *Eur. Phys. J. D*, **20**, 339 (2002).
78 J. Kohno, F. Mafuné, and T. Kondow, *Chem. Phys. Lett.*, **366**, 531 (2002).
79 "Atomic and Molecular Beam Methods," ed by G. Scoles, Oxford University Press, Oxford (1988), Vol. I, p. 190.
80 D. Brahat, O. Cheshnovsky, U. Even, N. Lavie, and Y. Magen, *J. Phys. Chem.*, **91**, 2460 (1987).
81 N. J. Turro, "Modern Molecular Photochemistry," Benjamin/Cummings, Menlo Park (1978).
82 S. H. Pine, "Organic Chemistry," 5th ed, McGraw-Hill Int., New York (1987).
83 Farhataziz and M. A. J. Rodgers, "Radiation Chemistry," VCH, New York (1987).
84 G. V. Buxton, C. L. Greenstock, W. P. Helman, and A. B. Ross, *J. Phys. Chem. Ref. Data*, **17**, 513 (1988).
85 M. J. Blandamer and M. F. Fox, *Chem. Rev.*, **70**, 59 (1970).
86 C. A. Woodward, M. P. Dobson, and A. J. Stace, *J. Phys. Chem. A*, **101**, 2279 (1997).
87 W. Lu and S. Yang, *J. Phys. Chem. A*, **102**, 825 (1998).
88 M. R. France, S. H. Pullins, and M. A. Duncan, *Chem. Phys.*, **239**, 447 (1998).
89 In fact, the hydration of Phe^+ proceeds via a stabilization of a hot intermediate species, $Phe^+ \cdot (H_2O)_1^{\ddagger}$, by a collision of another water molecule as

$$Phe^+ + H_2O \underset{k_2}{\overset{k_1}{\rightleftarrows}} Phe^+ \cdot (H_2O)_1^{\ddagger} \xrightarrow{k_3[H_2O]} Phe^+ \cdot (H_2O)_1. \quad \text{(a)}$$

If a steady state condition is fulfilled for the formation of $Phe^+ \cdot (H_2O)_1$, one obtains

$$-\frac{\Delta[Phe^+]}{\Delta t} = \frac{k_1 k_3 [H_2O]^2}{k_2 + k_3[H_2O]} \cdot [Phe^+], \quad \text{(b)}$$

where $\frac{d[Phe^+]}{dt}$ is approximated to be $\frac{\Delta[Phe^+]}{\Delta t}$. The value of $k_1[H_2O]$ is derived from Eq. (b) as

$$k_1[H_2O] = -\frac{\Delta I_P}{\Delta t \cdot I_P} \frac{\left(1 + \sqrt{1 + \frac{4k_1k_2}{k_3} \cdot \frac{\Delta t \cdot I_P}{\Delta I_P}}\right)}{2}. \quad \text{(c)}$$

The number density of water molecules in the cloud is estimated from k_1, k_2, and k_3 given as follows: The value of k_2 is estimated to be $\sim 10^3$ s^{-1} by RRK theory as

$$k_2 = A\left(\frac{E_i}{E_i + E_d}\right)^{s-1}, \quad \text{(d)}$$

where A, E_i, E_d, and s represent the frequency prefactor (4×10^{12} s^{-1}), the internal energy (assumed to be 300 K), binding energy of Phe^+ and H_2O (0.76 eV[57]), and the degree of freedom of $Phe^+ \cdot (H_2O)_1^{\ddagger}$ ($3 \times 17 - 6$), respectively. The values of k_1 and k_3 are estimated to be 7.3×10^{-16} and 7.2×10^{-16} m^3 $molecule^{-1}$ s^{-1}, respectively, from the Langevin rate constant (see text). By using these values, the value $[H_2O]$ is calculated. The calculated values of $[H_2O]$ by Eq. (c) deviate less than 1% from the values calculated by Eq. 49, and therefore one can regard the reaction (a) as the first-order reaction.

Award recipient

Jun-ya Kohno, born in Tokyo in 1969, received his B.S. degree in 1992 and his M.S. in 1994 from The University of Tokyo under the supervision of Professor Tamotsu Kondow. He worked in the Central Technical Research Laboratory of Nippon Oil Company, Ltd. for the study of lubricants between 1994 and 1998. Then he joined Genesis Research Institute, Inc. in 1998 as a member of research staff. He received his Ph.D. in 2000 from The University of Tokyo under the guidance of Professor Kaoru Yamanouchi. In 2000, he won the Award for Young Tribologists from the Japanese Society of Tribologists. His current research interest is focused on dynamics of reactions in solutions initiated by laser excitation.

Fumitaka Mafuné was born in 1966. He received his Ph.D. degree in chemistry from The University of Tokyo in 1994 under the supervision of Professor Tamotsu Kondow. He started his carrier as a research associate, Department of Chemistry, The University to Tokyo. After moving to Cluster Research Laboratory, Toyota Technological Institute in 1997, he was promoted to Lecturer in 1998 and Associate Professor in 2002. He was assigned as Associate Professor, Department of Basic Science, School of Arts and Sciences, The University of Tokyo in 2003. He won The CSJ Award for Young Chemists in 1998.

Tamotsu Kondow was born in 1936. He received his Ph.D. degree in chemistry from The University of Tokyo in 1967. He started his carrier as a research associate, Department of Chemistry, The University of Tokyo. He continued his study at Space Research Coordination Center, University of Pittsburgh between 1971 and 1973 as a research associate. After returning to Department of Chemistry, The University of Tokyo in 1973, he was promoted to Associate Professor in 1978 and to Professor in 1988. Concurrently with retiring from the Professor chair in 1997, he was assigned as the head of the newly started Cluster Research Laboratory, Toyota Technological Institute. He has more than 400 publications including original papers, reviews, and book contributions. His awards include the CSJ Award for Creative Work for 1986 and Humboldt Research Award for 2004.